Journal of Research
of the National
Bureau of Standards

The Journal of Research of the National Bureau of Standards features advances in measurement methodology and analyses consistent with the NBS responsibility as the nation's measurement science laboratory. It includes reports on instrumentation for making accurate and precise measurements in fields of physical science and engineering, as well as the mathematical models of phenomena which enable the predictive determination of information in regions where measurements may be absent. Papers on critical data, calibration techniques, quality assurance programs, and well characterized reference materials reflect NBS programs in these areas. Special issues of the Journal are devoted to invited papers in a particular field of measurement science. Occasional survey articles and conference reports appear on topics related to the Bureau's technical and scientific programs.

Comparison of Solid Density Standards Between IMGC and NBS

Anna Peuto

Istituto di Metrologia "G. Colonnetti," Strada delle Cacce 73, 10135 Turin, Italy

and

Richard S. Davis

National Bureau of Standards, Gaithersburg, MD 20899

Solid-object density standards developed independently by the Istituto di Metrologia "G. Colonnetti" (IMGC) and NBS, and traceable to SI units of length and mass, have been compared using a silicon transfer standard. Results agree to approximately 1×10^{-6}, which is conistent with the uncertainties assigned by the two laboratories.

Key words: density standards; hydrostatic weighing; international comparison; International System of Units; silicon; volume standards.

1. Introduction

The commonly adopted density standard is water. The main drawback of water as a reference standard is its reproducibility, which is difficult to check. The last international comparison of density measurement, involving eight major metrological laboratories [1][1], gave results which differed by as much as 13 parts per million (ppm) on the measurement of a stainless steel kilogram volume by hydrostatic weighing.

In classical hydrostatic weighing many sources contribute to the final uncertainty aside from the density of the reference liquid. Nevertheless, the adoption of a solid density standard allows the metrologist to overcome the problem of water reproducibility and to diminish the effect of other sources of error.

NBS began a program to establish a solid density standard in 1965 [2] and, more than 10 years ago, became the first laboratory to succeed in doing so [3]. The Istituto di Metrologia "G. Colonnetti" (IMGC) is among the laboratories which have later developed solid standards [4], following slightly different procedures but coming to the same result: a number of solid objects whose mass and volume are directly traceable to the SI mass and length standards.

No matter which procedure is adopted, measurement of the mass and of the linear dimensions, from which volume is computed, is a complex process, involving sophisticated techniques and accurate measurement of many influencing quantities.

Solid density standards can then be compared to liquid or solid samples through hydrostatic weighing, which again requires a fair deal of attention to sources of

---

About the Authors: Anna Peuto is with IMGC's mass and volume unit (Sezione Masse-Volumi) while Richard S. Davis serves with the NBS Length and Mass Division.

---

[1] Numbers in brackets indicate literature references.

error [5,6]. The best way of assessing the estimate of the uncertainty of both the standards and the procedure used is to have a comparison of standards through hydrostatic weighing.

We have completed such a comparison between IMGC and NBS using silicon crystals as transfer standards.

1.1 Plan of the Comparison

The NBS working standards of density are four 200-g silicon crystals, while IMGC's are three 1-kg spheres of glass-ceramic ($\rho \sim 2.5$ g/cm^3). A compromise had to be reached on the optimum size for the transfer standards and their number. We ultimately decided for maximum convenience of both laboratories to use two cylindrical silicon crystals of approximately 800 g each.

The silicon cylinders were fabricated at NBS from a single rod of commercially-grown, semiconductor-grade material. The rod had previously been ground to a diameter of approximately 7.5 cm. It was sawn twice to produce two cylinders of approximately 810 g. All edges of the cylinders were then bevelled. The cylinders were marked for easy identification by grinding one flat spot into the edge of the crystal henceforth referred to as X1 and producing two such flats in the second crystal, X2. Work damage was removed by etching the crystals in a bath of nitric and hydrofluoric acids [7]. The crystals were further etched to bring their masses to approximately 800.3 g (i.e., apparent mass against stainless steel of 8 g/cm^3 density = 800.0 g).

The transfer standards were to be compared by hydrostatic weighing to the solid density standards first at NBS, then at IMGC, and finally at NBS again.

We agreed on having each institute follow its own procedures for both the experimental process and the treatment of data. The comparison was meant to be a comparison of density measurements performed on the same basic principles but carried out in thoroughly independent ways, each result affected by the laboratory's own data analysis and by possibly different systematic influences.

The goal of the project was of course to verify the agreement of the final density values, the uncertainty estimate of both institutes being at the 1 ppm level. A strong motivation for such a verification is that the NBS density work has been used to help provide a measurement of N_A, the Avogadro constant. The density measurements, in fact, were the dominant uncertainty in the reported error budget. When that work was done, which was about 15 years ago, it was found that the measured volumes of steel spheres used to establish a working volume standard depended systematically on which of two methods had been used in their cleaning. The two results differed by about 2 ppm. No satisfactory explanation for the discrepancy having been found, it was decided to average the two results and assign an expanded uncertainty of 1 ppm [8]. This is a strategy often imposed upon metrologists because of practical constraints but it is, nonetheless, a solution which begs further study. The work reported here provides an independent check of the density scale used in the NBS determination of N_A.

2. IMGC Standards

The IMGC project for the realization of solid density standards started in 1978. The choice of shape and material, influenced by previous work at NBS, fell on spheres made of Zerodur^2, a glass-ceramic of very low thermal expansion coefficient ($\alpha \approx 10^{-8}$/K). The artifacts, produced for IMGC by an Italian optical firm, have masses slightly below 1 kg and diameters of about 90 mm. The material being inert in air and water, the spheres can be used in hydrostatic weighing. Three such spheres became IMGC's working density standard after measurement of their average diameter. The latter was obtained, for each sphere, by measuring the absolute value of two diameters at 90° and the diametral variations, for a family of nine planes 20° apart passing through each measured diameter [4,9].

To date, mass and volume measurements have been completed on three spheres, which are referred to as SP, S2 and S4. They are of different geometrical quality; SP and S4 have diameter variations not exceeding 0.2 μm and S2 has a maximum variation of 0.8 μm. Uncertainties of volume values are nonetheless estimated to be all within 0.7 ppm (this represents one standard deviation of the mean, 1 s_m).

Average diameter values are traceable to the length standard realized by means of an iodine ($^{127}I_2$) stabilized He-Ne laser, while mass values are traceable to the International Prototype Kilogram through stainless steel mass standards.

2.1 Plan of Comparison

Since the purpose of the project was the determination of the density of the two 800-g crystals by comparison with the three IMGC solid density standards, the five objects were weighed together in air and water cycles involving three objects at a time. From the weighings in air we obtained the mass difference between each pair of objects and between each object and a 1-kg stainless steel standard. Least-squares adjustment

218

of data yielded the masses of the three spheres and the two silicon cylinders.

From the weighings in bi-distilled water of known isotopic composition we obtained two types of results: first the values of all possible (10) volume ratios between the five objects; second, as an interesting check, the volume of the two crystals referred to water as a standard.

The original plan of the experiment, which provided for an equal number of measurements of all volume ratios, could not be carried out because of other commitments. Since IMGC standards were involved in many other density determinations during this comparison period, we obtained a very large amount of data on the mass and volume ratios of our own standards, but with smaller and unequal amounts of data on the crystals.

Rather than further delay the project's conclusion, we kept the data as they were and treated them by taking into account their different values of s_m.

2.2 Apparatus and Procedure

Both air and water weighings were performed with the same single-pan balance of 1-kg capacity and 10 div/mg sensitivity. All weighings were performed by comparison with calibrated stainless steel standards: the same 1-kg standard in the air weighings and the same 500 g and 100 g in the hydrostatic weighings were used for all the five objects, with additional masses to equalize loads.

An air buoyancy correction was applied to all weighings by calculating the air density through the formula recommended by International Committee for Weights and Measures (CIPM) [10], using measurements of atmospheric pressure, dew point, temperature, and estimate of CO_2 content from previous measurements in the lab; all instruments were calibrated against IMGC standards.

Hydrostatic measurements were performed using a loading mechanism quite similar to that of NBS; the suspension wire was of stainless steel (0.25 mm dia.) covered with platinum black. The vessel filled with bi-distilled water was placed in an insulated bath controlled by a circulation thermostat. The temperature was measured, via an AC double bridge, by two 25 Ω SPRT's, placed at the lower left and upper right of the artifact under test.

The water, of known isotopic composition [11], was not degassed: a series of tests carried out with an industrial dissolved-oxygen meter confirmed that at the moment of the weighings, some 48 hours after bi-distillation, the water can be assumed in equilibrium with atmosphere, i.e., saturated with gases.

Air weighings were double-substitution weighings, following a 5-reading format with two sensitivity determinations.

Hydrostatic weighings were performed in a slightly different way, following a 13-reading format, starting and ending with mass standards on the pan with and without the 500 mg sensitivity weight. Three observations were taken of the apparent mass of each of the objects involved, one reading taken with a smaller sensitivity weight, the three observations then being averaged to give a single value.

Smaller masses were added to the pan so that the readings relative to the three objects fall all within 1/4 of the optical scale.

From a 13-readings series two volume ratios (the third possible one being not independent) were obtained. During one series, temperature drift was usually kept within a few millikelvin and vertical gradient within 2 mK/10 cm.

All data were corrected for temperature drift and the crystal volumes were also corrected to a to 20 °C reference temperature (the water temperature was always kept within 0.2 K of 20 °C). The very different coefficient of thermal expansion of Zerodur and silicon is the only feature that has some influence, differences in compressibility, etc. being negligible.

3. Results

The whole experiment was meant to provide:
- the mass values of the two crystals, X1 and X2;
- the volume ratios of the two crystals to each of the IMGC standards and hence a final value of the crystal volumes; and
- the volume of the two crystals referred to water as a standard.

From the above one can compute the density of the crystals referred to IMGC standards (and compare it to NBS's value) and also referred to water, just as a check.

Let us examine the mass and volume ratios first.

3.1 Mass and Volume Referred to IMGC Solid Standards

The weighings in air of the five objects against the 1-kg standard and against each other provide 15 experimental equations that have been solved by the usual least-squares method.

From the hydrostatic weighings we obtained all 10 possible volume ratios as independent measurements and, again, least-squares adjusted values through a Connor-Youden procedure [12].

For both the mass and volume ratio measurements, we had sets with different numbers of measurements and different standard deviations. We then attributed to each

equation a weight inversely proportional to the variance of the mean of the corresponding experimental data, s_m^2.

Tables 1 and 2 give experimental results of the mass measurements and volume ratios, the number of measurements, standard deviation of the mean and least-squares adjusted values of the five masses and of the 10 volume ratios, together with the standard deviation of the fit and of the adjusted values.

Final uncertainties were estimated, following BIPM recommendations [13], as the combined uncertainties from type A and type B components.

Tables 3 and 4 list all sources of uncertainty and their influence on mass and volume ratio measurements together with the resulting combined uncertainty. The volumes of the three spheres, as computed from the interferometric measurement of their diameters, were not considered in the least-squares adjustment of volume ratios.

Since small discrepancies exist between hydrostatic and interferometric values of volume ratios for the IMGC standards, slightly different volume and density values for the silicon crystals can be computed, referred to each of the standards. These latter values are given in table 5, together with the average values and the combined uncertainty, where the uncertainty of the standards has been estimated as 0.7 ppm.

3.2 Water as a Reference

When water is taken as a reference a different philosophy must be adopted. Volume ratios are independent of the liquid used in the hydrostatic weighing, as long as

Table 1. Mass measurements (IMGC).

Object	Measured Values (g)	n	s_m (mg)	l.s. adjusted mass (g)	s_m of l.s. adjusted mass (mg)
X1	800.33240	13	0.04	800.33225	0.05
X2	800.30064	3	0.08	800.30070	0.07
S4	967.95836	13	0.03	967.95837	0.04
S2	979.68247	14	0.03	979.68249	0.04
SP	958.56833	30	0.03	958.56837	0.04

s of the fit=0.08 mg

Table 2. Volume ratios (IMGC).

R	Measured Ratio	n	s_m (10^{-6})	l.s. adjusted ratio	s_m of l.s. adjusted ratio
S4/SP	1.01232589	46	0.12	1.01232588	0.14
S4/X1	1.11341445	6	0.40	1.11341383	0.19
S4/X2	1.11345775	6	0.14	1.11345768	0.15
S2/S4	1.01065800	13	0.30	1.01065732	0.21
S2/SP	1.02311459	27	0.22	1.02311456	0.17
S2/X1	1.12527956	20	0.25	1.12527984	0.21
S2/X2	1.12532385	8	0.26	1.12532416	0.20
SP/X1	1.00985702	12	0.18	1.09985712	0.17
SP/X2	1.09990061	8	0.19	1.09990045	0.15
X1/X2	1.00003929	16	0.17	1.00003939	0.17

s of the fit=0.3×10^{-6}

Table 3. Uncertainty of mass measurements (IMGC).

Source of Uncertainty	Magnitude	Influence on Mass
1 kg standard	50 μg	50 μg
Other mass standard	70 μg	70 μg
Density of Air coming from:	0.28 μg/cm^3	68 μg
Pressure	16 Pa	
Dew point	0.3 K	
Temperature	25 mK	
CO$_2$ content	1×10^{-4}	
Formula	0.08 μg/cm^3	
Volume of unknown	0.4 mm^3	0.5 μg
Volume of 1 kg standard	0.9 mm^3	1 μg
Volume of other mass standards	30 mm^3	35 μg
Sensitivity reading	1 div	20 μg
	RSS	0.12 mg
	s_m	X1: 0.05 mg X2: 0.07 mg
Combined Uncertainty		0.14 mg

Table 4. Uncertainty of volume ratio measurements (IMGC).

Source of Uncertainty	Magnitude	Influence on Ratio Measurement (10^{-6})
Mass standard	195 μg	0.2
Volume of mass standards	90 mm^3	0.1
Density of air	0.28 μg/cm^3	0.03
Coefficient of thermal dilation of silicon	5×10^{-8}/K	0.01
Temperature drift	1 mK	0.2
Absolute temperature	1 mK	0.001
	RSS	0.3×10^{-6}
	s_m	0.2×10^{-6}
Combined Uncertainty		0.4×10^{-6}

220

Table 5. Density and volume of X1 and X2 referred to IMGC standards.

Standard	Density (20 °C) X1 (g/cm³)	X2 (g/cm³)	Volume (20 °C) X1 (cm³)	X2 (cm³)
S2	2.3290763	2.3290763	343.62646	343.61292
S4	2.3290783	2.3290782	343.62617	343.61264
SP	2.3290789	2.3290789	343.62608	343.61254
Average	2.3290778	2.3290778	343.62624	343.61270
S_m	0.0000008	0.0000008	0.00011	0.00011

Uncertainty of density measurements

Source of Uncertainty	Magnitude	Influence on Radio Measurement
Volume ratio	0.4×10^{-6}	0.9×10^{-6} g/cm³
Mass	0.14 mg	0.4×10^{-6} g/cm³
Density standard	0.7 ppm	1.6×10^{-6} g/cm³
	RSS	1.9×10^{-6} g/cm³ (0.8 ppm)
	S_m	0.8×10^{-6} g/cm³
Combined Uncertainty		2.0×10^{-6} g/cm³ (0.9 ppm)

its density can be considered near constant during weighings. Gas content, purity and absolute temperature of the water are not a problem when measuring volume ratios but are of the highest importance when water becomes the reference standard.

When doubts about water conditions arise, the weighings must be disregarded: thus some of the observations which could be considered when comparing volumes were disregarded when measuring volumes referred to water. We nonetheless came out with a fair amount of data on X1 and X2 volumes, measured in different samples of water.

Once again the number of measurements and the number of water samples are not the same for the two crystals, but the information is sufficient to check both crystals and confirm the tentative conclusion we have drawn on water, as prepared and analyzed at IMGC.

The volumes of X1 and X2 referred to water are given in table 6, as average results of weighings in the same water sample, together with the number of measurements and standard deviation of the mean. The temperature of the water was between 19.8 °C and 20.0 °C. The data were corrected for thermal expansion of silicon (ref. temp. 20 °C), isotopic composition [14], and gas content of water (-2.5×10^{-6} [15]).

Averaging all observations, as they can be considered to belong to the same set, we obtain a final value in very

good agreement with those referred to solid density standards.

The final uncertainty, given in table 7, is only slightly larger than in the case of the solid reference standards. However, there are influencing quantities (gas content, isotopic variations, contamination, etc.) for which either a rough estimate or no estimate at all can be made.

Only after a considerable number of hydrostatic weighings of the solid density standards were we able to assess our water reproducibility; the results on X1 and X2 provide a further check. We have found, in other experiments, maximum discrepancies of 3 ppm.

4. NBS Standards

The fundamental density work at NBS was carried out more than 10 years ago and has been well summarized in review papers [8,16]. Briefly, the volume of highly spherical steel balls was determined by interferometric measurements of ball diameter. Measurement of the mass of each ball then determined its density. It was assumed that the stability in density of the balls would be inferior to that of single-crystal silicon. Therefore, soon after the ball densities were determined, the balls were used to determine the density of four 200 g discs of single-crystal silicon. The transfer was made hydrostatically in a bath of fluorocarbon. Water could

Table 6. Volume of X1 and X2 referred to water (IMGC).

Water Sample	Volume of X1 (cm³)	n	S_m (mm³)	Volume of X2 (cm³)	n	S_m (mm³)
1 (19.8 °C)	343.62620	5	0.17			
2 (19.8 °C)	343.62600	5	0.08			
3 (19.9 °C)	343.62632	5	0.13			
4 (19.8 °C)				343.61332	5	0.13
5 (20.0 °C)	343.62638	8	0.07			
6 (19.9 °C)	343.62610	8	0.03	343.61268	8	0.06
7 (19.9 °C)	343.62628	7	0.08	343.61270	7	0.06
Average	343.62622	38	0.04	343.61285	20	0.08
Density	2.3290779 g/cm³			2.3290768 g/cm³		
Difference from density referred to solid standards	+0.1×10⁻⁶ g/cm³			−0.9×10⁻⁶ g/cm³		

not be used as the transfer fluid because it would have attacked the surface of the steel balls. The fluorocarbon fluid turned out to have many desirable properties compared with water—lower surface tension, higher density, larger appetite for gases. Its chief drawbacks are its higher thermal expansion coefficient and its poorer thermal conductivity.

This work was completed by 1972. The four silicon discs remain the NBS working standards of density.

4.1 Plan of Comparison

The objective of our measurements was the determination of the density of X1 and X2, using our four 200-g silicon discs as working standards. Similar to the measurements at IMGC, we measured the mass of the six objects by weighings in air after which the hydrostatic weighings were carried out.

The hydrostatic weighing and analysis were done as described in reference [5] using fluorocarbon as the transfer fluid. As a check, we also made several measurements using water as the transfer fluid. The water density was not known a priori to useful levels of accuracy because it was singly-distilled tap water of unknown isotopic composition.

In all the measurements, the volume ratios of four objects were determined in all six possible pairings. These data were collected in about three hours and constitute one "run." The four objects used were: X1, X2, and two groups of two discs each. The data from each run were analyzed by non-linear least-squares fitting using the total volume of the four discs as a restraint. The computed difference of the two disc-summations and the standard deviation of the least-squares fit were used as process controls.

Seven runs were carried out prior to sending X1 and

X2 to IMGC. Four of these used fluorocarbon as a transfer fluid and three used water. Two additional runs in fluorocarbon were made after the crystals returned to NBS.

Table 7. Uncertainty of measurements referred to water (IMGC).

Source of Uncertainty	Uncertainty	Influence on Volume Measurement (mm³)
Mass of crystal	0.13 mg	0.13
Mass of standards in hydro weigh.	0.17 mg	0.17
Volume of mass standards	84 mm³	0.10
Sensitivity reading	1 div	0.02
Height difference	0.1 m	0.01
Thermal dilation of silicon (a)	5×10⁻⁸/K	0.00
Temp. difference from 20 °C	1 mK	0.00
Density of air	0.28 μg/cm³	0.08
Density of water coming from:	7.3×10⁻⁷ g/cm³	0.25
Temperature	1 mK	
Gas content	20%	
Isotopic abundance	2×10⁻⁶	
Pressure	16 Pa	
Depth	1 cm	
RSS		0.35
S_m		X1: 0.04 X2: 0.08
Combined Uncertainty		0.36 mm³ (1 ppm)

4.2 Apparatus and Procedure

The mass of each 200-g disc was determined by double substitution against a 200-g stainless steel working standard. Measurements were made on a modified single-pan balance having a standard deviation of 12 μg. The two 800-g crystals, X1 and X2, were weighed on a single-pan kilogram balance having a standard deviation of 25 μg. Calibrated stainless steel weights were added to the silicon crystals until their apparent mass equalled that of two of our stainless steel 1-kg standards. The four objects of nearly-equal apparent mass were then intercompared by double-substitution, weighing in all six possible pairings. Standard least squares techniques were used to assign mass values to the unknown objects.

Buoyancy corrections were made using the same equation for the density of moist air as was used at IMGC [10]. Inputs to the equation were obtained from a thermometer and hygrometer mounted in the balance case and from an aneroid barometer placed on an adjacent bench. The ambient level of carbon dioxide was assumed to be that measured previously during surveys of our laboratory.

All hydrostatic measurements were as described in [5]. Our bath chamber below the balance was enlarged slightly to accommodate X1 and X2, since their volumes are larger than any object we have previously measured.

The hydrostatic weighings were analyzed in a slightly different way than in previous work. A hydrostatic weighing of an object, A, proceeds as follows:

I_1: balance pan unloaded
I_2: A on pan in fluid
I_3: A on pan in fluid, S on pan in air
I_4: S on pan in air
I_5: balance pan unloaded,

where S is a 20 mg sensitivity weight of known mass. The set I_1 to I_5 are balance indications. The balance used is a single-pan device with calibrated built-in weights and a 100 mg optical scale that can be read to the nearest 20 μg. Thus each I_i is the sum $D_i + O_i$ where D_i is the combination of calibrated built-in weights used and O_i is the reading on the optical scale. Tare weights are used to ensure that $D_1 = D_4$, $D_2 = D_3$, and O_1 and O_2 are within one half of the optical scale range.

In the past, we have estimated the contribution of the optical readings to the apparent mass of A in the bath fluid as

$$\frac{M_s'}{2}\left(\frac{O_2-O_1}{O_3-O_2}+\frac{O_3-O_4}{O_4-O_5}\right) \qquad (1)$$

where M_s' is the mass of S reduced by the buoyant effect of air. The drift during the five observations is estimated by

$$\frac{M_s'}{2}\left(\frac{O_2-O_1}{O_3-O_2}-\frac{O_3-O_4}{O_4-O_5}\right) \qquad (2)$$

In this work, we replace eqs (1) and (2) with

$$\frac{M_s'}{2}\left(\frac{O_2-O_1+\frac{1}{4}(O_1-O_5)}{O_4-O_5-\frac{1}{4}(O_1-O_5)}+\frac{O_3-O_4-\frac{1}{4}(O_1-O_5)}{O_4-O_5-\frac{1}{4}(O_1-O_5)}\right) \text{(1a)}$$

and

$$\frac{M_s'}{2}\left(\frac{O_2-O_1+\frac{1}{4}(O_1-O_5)}{O_4-O_5-\frac{1}{4}(O_1-O_5)}+\frac{O_3-O_4-\frac{1}{4}(O_1-O_5)}{O_4-O_5-\frac{1}{4}(O_1-O_5)}\right). \text{(1b)}$$

Equations (1a) and (1b) differ most from (1) and (2) when $V_A\dot{\rho}_L$ is a large number, where V_A is the volume of A and $\dot{\rho}_L$ is the time derivative of the density of the bath fluid. Generally, $\dot{\rho}_L = (\partial\rho_L/\partial T)\dot{T}$. We also assume a linear drift in T, the bath temperature. In (1) and (2), the quantity $(M_s'/2)\cdot(1/(O_3-O_2))$, which is supposed to be an estimate of balance sensitivity, will contain a significant error if $V_A\dot{\rho}_L$ is large. The penalty for this error falls heaviest on those measurements for which (O_2-O_1) is the largest percentage of full-scale. Equations (1a) and (1b), on the other hand, estimate balance sensitivity independent of the volume of the object being weighed. The quantity $(1/4)(O_1-O_5)$ is used to eliminate the small effect of $\dot{\rho}_L$ on the volume of the submerged balance pan. Drift in the fluid density is still measured by comparing the magnitude of (1b) with zero. We may note that the quantity (1a), in addition to random errors, will now be systematically biased by the amount ϵV_A, where ϵ is the increase in bath density between successive measurements. The effect of this bias can be made negligible by establishing a maximum drift criterion and monitoring the quantity (1b) for each group of measurements.

The use of (1a) also means that non-linearities in the optical scale readings are not accounted for, but experience has shown that the non-linearities are small compared with the effects of temperature drift during a reading.

It is worth noting that in analyzing a large quantity of data using both schemes for data reduction, virtually identical final results for every run were obtained. The difference is that the computed standard deviations of the least squares fits were, on occasion, significantly less using the modified scheme.

5. Results

The results of the NBS measurements are shown in tables 8–11. In table 8, the "first set" of measurements was made at NBS prior to sending X1 and X2 to IMGC. The "second set" of measurements was made after the

223

Table 8. Mass measurements (NBS).

Object	Measured Mass, 1st Set (g)	Measured Mass, 2nd Set (g)	Estimated s_m (μg)	No. of Deg. of Freedom
X1	800.331922	800.331839	35	9
X2	800.300387	800.300375	35	9
Disc 1	200.420702		22	2
Disc 2	199.763720		22	2
Disc 3	200.006331		22	2
Disc 4	199.426629		22	2

Table 9. Uncertainty in mass measurements (NBS).

Source of Uncertainty	Magnitude	Influence on Unknowns (μg)	Influence on Standard Discs (μg)
1 kg standard (stainless steel)	50 μg	40	20
200 g standard	23 μg	23	23
Density of air coming from:	0.40 $\mu g/cm^3$	97	49
Pressure	13 Pa		
Relative humidity	3%		
Temperature	50 mK		
CO_2 content	1×10^{-4}		
Formula	0.08 $\mu g/cm^3$		
Volume of unknowns	1 ppm	0.4	0.2
Volume of 1 kg standard	1.3 mm^3	1.2	0.6
Volume of 200 g mass standard	1.3 mm^3	1.5	1.5
Sensitivity reading	1 div	20	20
RSS		109	61
s_m		35	22
Total Uncertainty		115 μg	65 μg

return of the transfer standards from IMGC. It is possible that X1 has lost mass during its use although the difference is just at the level of significance (see table 9) even accounting for uncertainties which are common to both sets of measurements. The masses of the four discs have been stable for a number of years. An accident in 1978 involving Disc 4 caused the last change in any of the measured masses.

In table 10, runs 8 and 9 were made subsequent to the return of X1 and X2 to NBS. The masses obtained in the second set of table 8 were used for these two runs. No obvious systematic behavior was observed so the results were pooled with equal weight assigned to each run.

In table 10, it is worth noting the differences in propagated error as a function of transfer fluid. The temperature of the bath need not be known because X1, X2 and the four standard discs have identical temperature coefficients. The other zeros in table 10 are a result of the standards and unknowns being almost identical in density. That is, any type B error which has the effect of changing I_x and I_s (see below) to KI_x and KI_s (where $K \approx 1$) propagates as an error in V_x or D_x which is pro-

Table 10. Results of nine runs (NBS).

Run No.	Transfer Fluid	Grouping of Standard Discs	Fitted Volumes (cm^3) X1	Fitted Volumes (cm^3) X2	Estimated s_m, 3 Deg. of Freedom (mm^3)	Computed Densities (g/cm^3) @ 20 °C X1	Computed Densities (g/cm^3) @ 20 °C X2
1	Fluorocarbon	2+4, 3+5	343.625187	343.611593	0.113	2.3290835	2.3290839
2	Fluorocarbon	2+3, 4+5	343.625692	343.612283	0.090	2.3290801	2.3290792
3	Fluorocarbon	2+3, 4+5	343.625710	343.612123	0.054	2.3290799	2.3290803
4	Fluorocarbon	2+3, 4+5	343.625490	343.612017	0.051	2.3290814	2.3290810
5	Water	2+4, 3+5	343.626419	343.612648	0.143	2.3290754	2.3290770
6	Water	2+3, 4+5	343.625750	343.612266	0.041	2.3290800	2.3290796
7	Water	2+3, 4+5	343.625753	343.612298	0.076	2.3290800	2.3290794
8	Fluorocarbon	2+4, 3+5	343.625693	343.612234	0.112	2.3290803	2.3290800
9	Fluorocarbon	3+5, 2+4	343.625792	343.612358	0.078	2.3290796	2.3290791
		Average	343.625721	343.612202		2.3290800	2.3290799
		s_m	0.000108	0.000095		0.0000007	0.0000006

Table 11. Uncertainties in hydrostatic measurements (NBS).

Source of Uncertainty	Magnitude	Influence on V_x		Influence on D_x	
		Fluorocarbon (mm³)	Water (mm³)	Fluorocarbon (μg/cm³)	Water (μg/cm³)
Mass of two standard discs	65 μg	0.018	0.074	0.10	0.50
Density of two standard discs (Ds)	2.21 μg/cm³	0.326	0.326	2.21	2.21
Calibration of of built-in weights on hydrostatic balance (Type B)	15 μg/100g	~0	~0	~0	~0
Mass of unknowns, X1 and X2	115 μg	0.065	0.115	0.11	0.44
Sensitivity of hydrostatic balance	20 μg	0.016	0.028	0.11	0.19
Bath temperature	2 mK	~0	~0	~0	~0
Density of air	0.40 μg/cm³	~0	~0	~0	~0
	RSS	0.333	0.355	2.22	2.32
	s_m	0.107	0.107	0.72	0.72
	Total Uncertainty	0.350 mm³ (1.02 ppm)	0.370 mm³ (1.09 ppm)	2.33 μg/cm³ (1.00 ppm)	2.43 μg/cm³ (1.04 ppm)

portional to $(D_x - D_s)/\rho_L$, where ρ_L is the density of the bath fluid. In fact, calibration of the built-in weights was a major contribution to the error budget reported in [3] because in that work the volume standards were made of density 7.8 g/cm³ material and the unknowns were silicon. Note also that we are treating uncertainty in the air density during mass measurements and hydrostatic measurements as uncorrelated. This is because the measurements were made on different balances in different rooms with different thermometers, barometers, etc. This choice has little effect on the final uncertainty assignment, although the method used is the more conservative because an error in air density systematic to all mass measurements would have no effect on the resulting assignment of density.

6. Discussion

In comparing results between NBS and IMGC, one must look at the starting premises of the two laboratories. NBS assumes that the *densities* of its four silicon discs are known whereas IMGC assumes that the *vol-*umes of its three Zerodur spheres are known (or that the density of water is known when water is the standard). This leads to the following schematic equations for obtaining final results:

	NBS	IMGC	
STANDARD:	discs	spheres	water

$$V_x =: \qquad \frac{M_s}{D_s}\frac{M_x - I_x}{M_s - I_s} \qquad V_s\frac{M_x - I_x}{M_s - I_s} \qquad \frac{M_x - I_x}{\rho_w}$$

$$D_x =: \qquad D_s\frac{M_s - I_s}{M_s}\frac{M_x}{M_x - I_x} \qquad \frac{M_x}{V_s}\frac{M_s - I_s}{M_x - I_x} \qquad \frac{M_x}{M_x - I_x}\rho_w$$

where the symbols have the following meanings:

V_x: volume of unknown
V_s: volume of standard
M_x: mass of unknown
M_s: mass of standard

225

D_x: density of unknown
D_s: density of standard
ρ_W: density of water
I_x: $M_x - \rho_L V_x$ (apparent mass of unknown in fluid)
I_s: $M_s - \rho_L V_s$ (apparent mass of standard in fluid)
ρ_L: density of transfer fluid

D_x(NBS) and V_x(IMGC) are assumed known prior to the measurements reported here (we will defer discussion of the IMGC measurements based on water). Thus, for instance, while D_x(NBS) and V_x(IMGC,V_s) are measured independent of the SI unit of mass, V_x(NBS) and D_x(IMGC,V_s) do depend on the SI mass unit as presently realized in each laboratory. Other dependencies differ among the various measurement schemes as will be discussed presently.

Before examining possible discrepancies further, it is useful to compare those results of the two laboratories which should be almost independent of the mass, volume, or density scales used but, rather, depend only on experimental procedures. Such a measure is provided by a comparison of the ratio V_{X1}/V_{X2} measured by the two laboratories:

	V_{X1}/V_{X2}	s_m
IMGC:	1.00003939	0.00000017
NBS:	1.00003940	0.00000014

Based on the mean standard deviations we would expect agreement to about 0.2 ppm. The observed agreement of 0.01 ppm is well within these limits.

The densities reported by IMGC are, however, systematically lower than those of NBS by about 1.0 ppm. The volumes reported by IMGC for X1 and X2 are systematically higher by 1.4 ppm than those reported by NBS.

Although these discrepancies are by no means serious, given the claimed accuracies of the two laboratories at the estimated one standard deviation (1σ) level of accuracy, it is nevertheless useful to examine the possible sources for the slight offsets. In fact, one immediately notices that the masses of X1 and X2 reported by the two laboratories are discrepant by an average of 0.34 mg (0.43 ppm). Assuming the IMGC values to be correct, the NBS values for D_x and V_x would shift toward the IMGC values by 0.3 ppm and 0.8 ppm respectively if "corrected" for the mass error. On the other hand, if the NBS values were correct, the IMGC values for D_x and V_x would shift toward the NBS values by 0.6 ppm and 1.1 ppm for both types of measurements (i.e., spheres or water used as standards). The difference in shifts is due to the heavy reliance on fluorocarbon ($\rho \sim 1.8$ g/cm^3) as transfer fluid at NBS compared with

the exclusive reliance at IMGC on water ($\rho \sim 1.0$ g/cm^3) as either transfer fluid or standard[3].

It might be tempting, then, to attribute most of the observed discrepancies in V_x and D_x to the mismeasurement of the mass of X1 and X2 at one of the laboratories were it not for the fact that the Zerodur spheres and/or the silicon discs used as standards in the two laboratories would almost certainly be subject to the same systematic error. Such an error could arise from mass standards or from faulty evaluation of the density of air. If the standards and unknowns were both subject to the same systematic error, a "correction" at NBS would leave the values of D_x unchanged but would shift V_x closer to the IMGC value by 0.5 ppm. A similar "correction" at IMGC would move results farther from NBS by 0.6 ppm and 0.1 ppm for the case of Zerodur spheres used as standards; the results using water as standard would shift closer to NBS values by 0.6 ppm and 1.1 ppm. All these shifts can be estimated by propagating changes through the schematic equations given above.

Aside from the discrepant mass values, the systematic difference in density measurements might of course be due to the volume/density standards. In fact, among IMGC density measurements those referred to one of the spheres (S2) are lower than the others by about 1 ppm. S4 and SP are in much better agreement with NBS values (0.6 ppm). Discrepancies are still not significant compared to the uncertainties attributed to the standards, so that we considered all IMGC measurements in the final computation. Besides, IMGC standards were recently involved in a comparison with PTB sponsored by the European Economic Community (EEC): the results are still to be published but it might be useful here to note that the best agreement was obtained for S2, so that there is no evidence of this standard being mismeasured.

As for now, density measurements of 1 ppm uncertainty agreeing within 1 ppm are a satisfactory result. Separate inquiries should be carried out on each single cause of discrepancy to obtain both a better agreement and a smaller uncertainty.

7. Conclusions

The mass and volume assignments to the transfer standards, X1 and X2, made by IMGC and NBS agree to at worst 1.5 ppm, average density values agreeing to 0.9 ppm. Each laboratory assigns an uncertainty of about 1

---

[3] In fact, the measurements made at NBS which used water as the transfer fluid would shift by 0.6 ppm and 1.1 ppm while those using fluorocarbon would shift by 0.2 ppm and 0.6 ppm. It is interesting to note that no systematic differences in the water and fluorocarbon measurements at NBS were observed.

ppm so that the observed agreement is good. We note a larger than expected discrepancy in the assignment of mass to X1 and X2. Resolution of this discrepancy might improve volume agreement by as much as 1.1 ppm or worsen agreement by as much as 0.6 ppm.

While we cannot resolve the cleaning anomaly which was observed during the NBS work which established its volume standard, we can at least confirm that the uncertainty which NBS ultimately placed on its measurements is a reasonable one. Thus the uncertainty which these measurements brought to the measurement of the Avogadro constant by Deslattes et al. is also confirmed.

References

[1] Bonhoure, A., and G. Girard, CIPM Proc. Verbaux, 2nd Series **31**, 51–53 (1963).

[2] Bowman, H. A.; W. Gallagher and R. M. Schoonover, 20th Annual Conference of ISA, 1965, Preprint No. 14.8-4-65.

[3] Bowman, H. A.; R. M. Schoonover and C. L. Carroll, J. Res. NBS **78A**, 13–40 (1974).

[4] Peuto, A.; A. Sacconi, R. Panciera, W. Pasin, and M. Rasetti, in *Precision Measurement and Fundamental Constants II*, Natl. Bur. Stand. Spec. Publ. 617, B. N. Taylor and W. D. Phillips, eds. 449–459 (1984)

[5] Bowman, H. A.; R. M. Schoonover and C. L. Carroll, Metrologia **10**, 171–121 (1974).

[6] Peuto, A.; S. Pettorruso and M. Rasetti, *Proc. 2nd Symposium of IMEKO-TC8*, Budapest, Hungary, 305–315 (1983).

[7] Schoonover, R. M., Notes on the Preparation of Silicon Density Artifacts, NBSIR 76-1019 (1976).

[8] Deslattes, R. D., Proc. of Course LXVIII, *Metrology and Fundamental Constants*, Enrico Fermi Summer School of Physics, Varenna, Italy, 1976, Soc. Italiana di Fisica, Bologna, 38–113 (1980).

[9] Sacconi, A.; R. Panciera and W. Pasin, Proc. Intl. Symp. on the Meas. of Geometrical Quantities (ISMQ), Beijing, 1982 (in press).

[10] Giacomo, P., Metrologia **18**, 33–40 (1982).

[11] Guzzi, G. Euratom-Ispra, private communication.

[12] Connor, W. S., and W. J. Youden, J. Res. Natl. Bur. Stand. **53**, 114–116 (1954).

[13] BIPM Working Group on the Statement of Uncertainties. Recommendation INC-1 (1980). See Metrologia **17**, 73 (1981).

[14] Girard, G., and M. Menaché, Metrologia **7**, 83–87 (1971).

[15] Bignell, N., Metrologia **19**, 57–59 (1983).

[16] Deslattes, R. D., Ann. Rev. Phys. Chem. **31**, 435–461 (1980).

Production Rates
for Oxyfluorides SOF$_2$, SO$_2$F$_2$, and SOF$_4$
in SF$_6$ Corona Discharges

R. J. Van Brunt

National Bureau of Standards, Gaithersburg, MD 20899

The most abundant, long-lived stable gaseous species generated by corona discharges in SF$_6$ gas containing trace levels of O$_2$ and H$_2$O are the oxyfluorides SOF$_2$, SO$_2$F$_2$, and SOF$_4$. Absolute energy and charge rates-of-production of these and the minor products SO$_2$, OCS, and CO$_2$ have been measured at different total gas pressures from 100 kPa to 300 kPa and for discharges of different current, power, and polarity. Oxyfluoride yields for SF$_6$/O$_2$ mixtures containing up to 10% O$_2$ have also been measured. The results indicate that oxyfluoride production is not controlled by the concentrations of either O$_2$ or H$_2$O at levels below about 1%, and the rate controlling factor is the dissociation rate of SF$_6$ in the discharge. The discharge current and time dependence of the production rates are discussed in terms of gas-phase mechanisms that have been proposed to explain previous observations of electrical, thermal, and laser-induced decomposition of SF$_6$ and SF$_6$/O$_2$ mixtures. Upper limits on the total SF$_6$ decomposition rate in low-current discharges have been estimated. Details of the chemical analysis procedures are given, and application of the results to the design of chemical diagnostics for SF$_6$-insulated, high-voltage apparatus is discussed.

Key words: corona discharges; decomposition rates; production rates; SF$_6$; SF$_6$/O$_2$ mixtures; SOF$_2$; SO$_2$F$_2$; SOF$_4$; sulfurhexafluoride; sulfurylfluoride; thionylfluoride; thionyl tetrafluoride.

1. Introduction

The decomposition of gaseous SF$_6$ leading to formation of the oxyfluorides SOF$_2$(thionylfluoride), SO$_2$F$_2$(sulfurylfluoride), and SOF$_4$(thionyl tetrafluoride) as major stable gaseous end products has previously been observed under a wide range of experimental conditions. These include: 1) oxidation of SF$_6$ in O$_2$ induced by exploding metals [1];[1] 2) decomposition

---

---

[1] Numbers in brackets indicate literature references.

of SF$_6$ on metal surfaces by direct heating [2]; 3) high-power, laser-initiated dissociation of SF$_6$ and SF$_6$/O$_2$ mixtures [3–5]; 4) shock-tube pyrolysis of SF$_6$/O$_2$ mixtures [6]; 5) low-pressure rf and microwave discharges [7–10]; 6) high-pressure arcs [11–18]; 7) spark discharges [19–22]; and 8) corona and glow type discharges such as those considered here [14,18,23–26]. Precluding possible catalytic influences of metal vapors and surface reactions, it might be expected that, although the initial dissociation mechanisms and the degree of gas dissociation in these cases are quite different, the basic subsequent gas-phase chemical processes that yield oxyfluorides should be similar. The relative yields of SOF$_2$, SO$_2$F$_2$, and SOF$_4$, however, can depend on the availability of oxygen and the degree to which the SF$_6$ molecules are dissociated, e.g., as determined by gas temperature or discharge power level. Generally as gas pressure, temperature, or discharge power increases, SOF$_2$ production is observed to become more dominant

[1,14,16,19]. At lower pressures, temperatures, or discharge power levels, SOF_4 often dominates [1,3,8–10], and when O_2 is added to the gas, it is noted that [3,15] both SO_2F_2 and SOF_4 increase relative to SOF_2.

Most of the earlier experimental work on decomposition of SF_6 or SF_6/O_2 focused on the problem of identifying the final by-products or intermediate ion and neutral species (also see refs. [27–30]). There have been only a few attempts to determine absolute yields for the electric-discharge-generated by-products, and these were performed under conditions for which the discharge could not be easily controlled or quantitatively characterized, namely for arcs [15,18], sparks [20,22], and 60-Hz ac corona [18]. The motivation of the present work is to provide data on the absolute yield of the oxyfluorides from SF_6 in the presence of small quantities of O_2 and H_2O under steady, dc-corona discharge conditions which could be readily characterized and controlled. The measurements reported here have been made for different gas and discharge conditions selected to help elucidate the predominant mechanisms of oxyfluoride formation.

Quantitative data on oxyfluoride production are also needed to design chemical diagnostics for SF_6-insulated high-voltage apparatus in which corona or partial discharges could occur [31–32]. The formation of the oxyfluorides is accompanied by production of highly reactive species such as free fluorine and HF. These species can cause serious damage to conductors and solid insulating materials present in practical systems [33–36]. Although most gas-insulated systems are designed to be free of internal discharges, low-level partial discharges similar to the corona phenomena considered here may be unavoidable, and in some applications, like high-energy electrostatic accelerators [26], continuous corona discharges are frequently maintained during normal operation. The highly reactive products of a discharge do not remain in the gas for long and are consequently difficult to detect. Their level of production, however, could be inferred indirectly from measurements of oxyfluoride content, provided that: 1) the production rates for the oxyfluorides are known, and 2) the connection between oxyfluoride and corrosive species production is understood. The results of the present study provide further insight into the latter item as well as data for the former.

Although the rate data presented here either include or are consistent with those that were previously reported from our laboratory [37–38], the measurements have been extended to a wider range of conditions. Moreover, the present results are expressed in a way deemed to be more useful in the design of chemical diagnostics for practical systems and are thus intended to supplant the earlier data.

2. Definitions of Production Rates

Production rates are usually specified in terms of change in the quantity of substance per unit of time, denoted here as dc/dt. This rate is determined by the rates of the reactions and concentrations of the reactants involved in formation of the particular species of interest. For electric discharge-generated products, it is more useful to express the rates in terms of either quantity generated per unit of energy dissipated (r_u) or per unit of charge transported in the discharge gap (r_q). These are related to the time rate-of-production by

$$dc/dt = p(t)r_u, \text{ and } dc/dt = i(t)r_q, \quad (1)$$

where $p(t)$ and $i(t)$ are respectively the instantaneous discharge power and current. The net quantity of a substance generated in a discharge of duration t' is then given either by

$$c(t') = \int_0^{t'} i(t)r_q[i(t)]dt \quad (2a)$$

or

$$c(t') = \int_0^{t'} p(t)r_u[p(t)]dt \quad (2b)$$

where it is assumed that in general r_q and r_u depend on $i(t)$ and $p(t)$, respectively. Stable gaseous products generated in a localized discharge will usually diffuse rapidly throughout the volume in which the gas is contained so that the concentration observed will be given by $c(t')/V_s$, where V_s is the volume of the system. If one knows the volume of the system, the production rates, and level of discharge activity specified by either $i(t)$ or $p(t)$, one can then use eq (2a) or (2b) to predict the concentrations of the by-products which can be observed after a given time.

The preference for either r_q or r_u is determined by the predominant dissociation mechanism and by variations of these with either current or power dissipation respectively. In the case of high-current, arc-type discharges in which heating of the gas is important and thermal dissociation dominates, the quantity r_u is preferred because it is found [15,18] to be relatively constant, i.e., $dc/dt \propto p(t)$. However, for cold, low-current discharges such as corona, in which the dissociation of the gas is primarily governed by electron collision processes, r_q is more useful for predicting by-product buildup in practical systems and for interpreting results of measurements as described here.

Examples of oxyfluoride energy or charge rates-of-production estimated from data that have previously been reported [15,18,39] for SF_6 are shown in table 1. In addition to these results, Castonguay [22] recently re-

230

Literature Reference	Discharge Type	Electrode Material	Production Rates			units
			SOF_2	SOF_4	SO_2F_2	
Sauers et al. [39]	spark	S.S.*	1.8	0.22	0.021	(nmoles/J)
Boudene et al. [15]	arc	S.S.*	24	0.3	0.8	(nmoles/J)
Boudene et al. [15]	arc	Ag	0.4	0.4	0.3	(nmoles/J)
Boudene et al. [15]	arc	Cu	8.12	0.3	0.5	(nmoles/J)
Chu et al. [18]	corona	Al	(370–850)	–	(190–420)	(μmoles/C)

*Stainless steel

ported a total SF_6 decomposition rate in a 60 W arc employing stainless steel electrodes to be about 7 to 8 nmoles/J. In a much earlier work, Waddington and Heighes [24] estimated the total gaseous by-product production rate in SF_6 point-plane partial discharges to be about 2 μmoles/J. This estimate disagrees significantly with the results in table 1 and is not consistent with either the data or the theoretical upper limit on SF_6 decomposition to be discussed here.

3. Measurement Method

3.1 Discharge

The electric discharge used for this investigation was a highly localized, low-current, point-plane corona. Characteristics of this type of discharge have previously been described [40,41]. A schematic of the experimental arrangement is shown in figure 1. Polished stainless steel electrodes were used in a 3.7 liter cell with a point-to-plane gap of 1.5 cm and point radius-of-curvature at the tip of about 0.08 mm. The cell contained a static gas sample which was maintained at room temperature (~300 K).

The zone of ionization, assumed here to coincide with the chemically active region, is confined to the immediate vicinity of the point electrode tip due to the highly divergent nature of the electric field. It is estimated from consideration of the field [40] that the active region extends a distance from the point which is no more than 2% of the total point-to-plane gap spacing, i.e., no more than about 4 point-electrode tip radii. The extent of the active region and the ion drift volume were therefore small compared to the relatively inactive volume of gas contained in the discharge cell.

A continuous corona was generated with a high-voltage dc supply that could be operated at either polarity, and consistent with the usual convention [4], the designated sign of the discharge refers to the potential of the point electrode relative to the plane. The voltage across the cell was continuously monitored and adjusted to maintain a constant average discharge current (see fig. 2). During a typical experiment of 20 to 70 h duration it was usually necessary to initially decrease and then gradually increase the voltage in order to keep the current constant. The average currents could be kept constant for the positive and negative discharges to within ±1% and ±4% respectively. The adjustments in
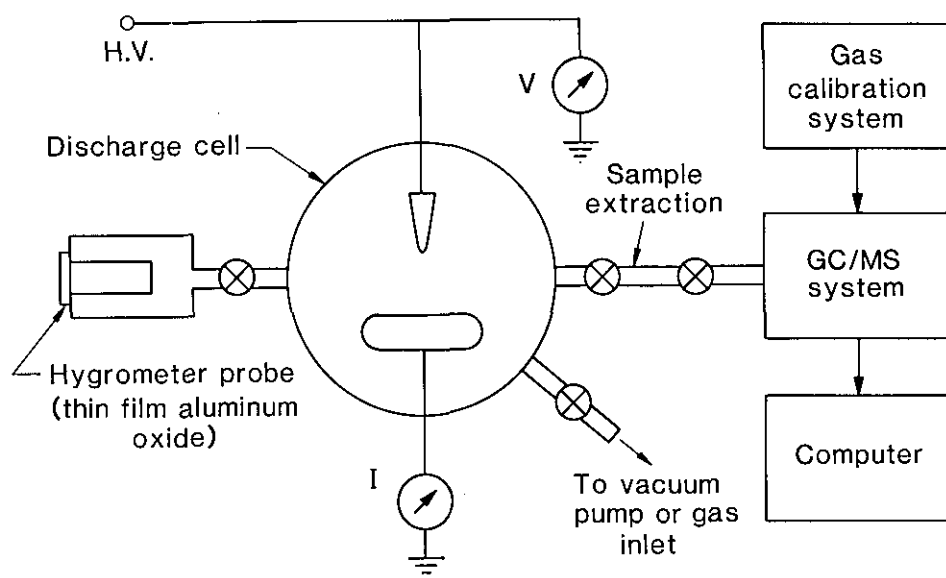
Figure 1-Experimental arrangement.

Negative corona — — 8 µ A

Positive corona — — 8 µ A

— 0

— 0

|← —————— 1.5 h —————— →|
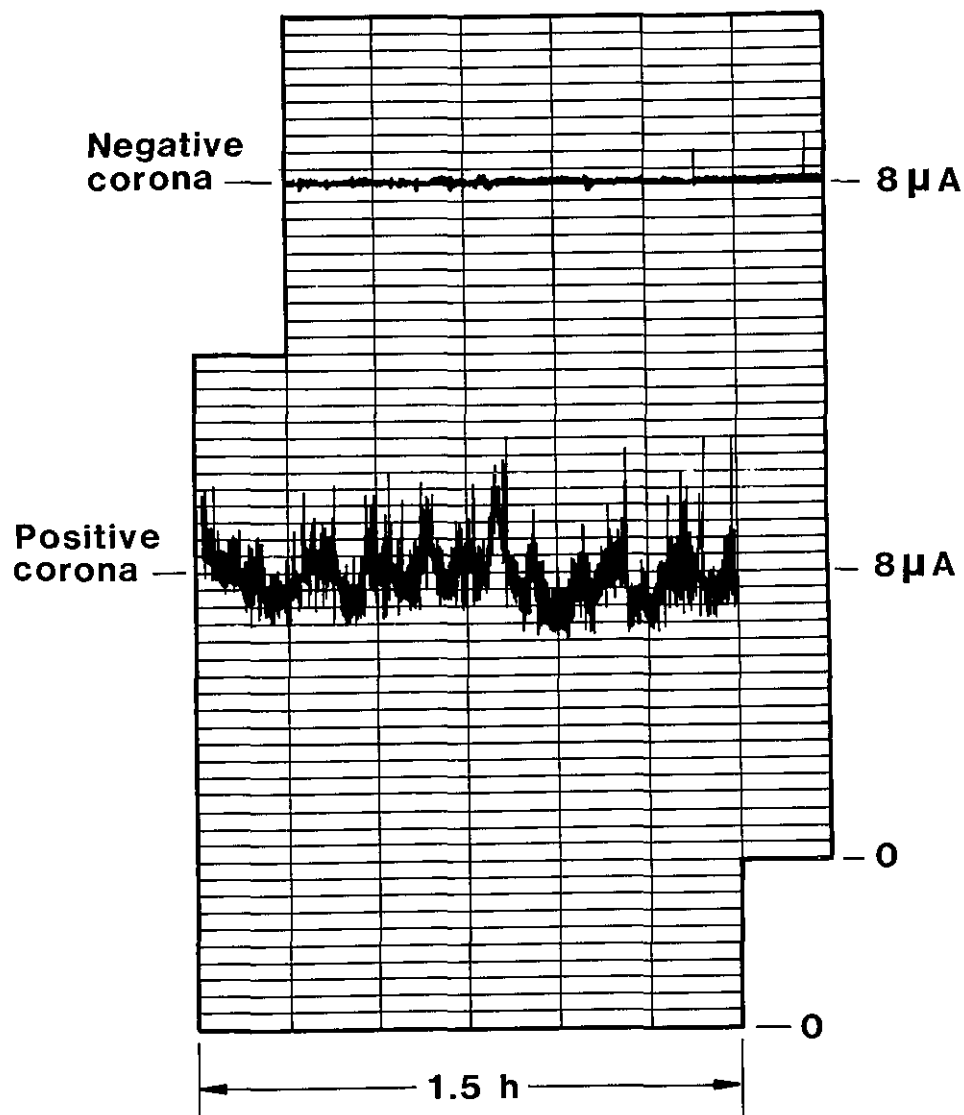
Figure 2-Examples of recordings showing the typical behavior of discharge current versus time for positive and negative corona discharges at comparable average current levels ($i_{av}=8.0$ µA) for a period of 1.5 h.

voltage were necessary because of the discharge-produced changes in both the gas composition and the point-electrode surface characteristics that influenced the ionization rate in the gas. The marked effects of "electrode conditioning" and trace levels of water vapor on the discharge voltage-current characteristics in SF$_6$ have previously been noted [37,40,42].

Figure 2 shows typical recordings of outputs from the electrometer used to measure the discharge current. At any time t', the accumulated energy dissipated and net charge transported in the discharge were computed respectively using

$$u(t')=i_{av} \int_0^{t'} V(t)dt,$$ (3)

and

$$Q(t')=i_{av}t',$$ (4)

where i_{av} is the time-averaged current as determined from the electrometer output and $V(t)$ is the instantaneous voltage drop across the cell.

3.2 GC/MS measurements

The chromatographic method and gas chromatograph-mass spectrometer system (GC/MS) used for gas analysis was similar to that described by others [7,9,14-15] for observation of neutral decomposition products in SF$_6$. The GC/MS was a modified commercial instrument consisting of a Teflon[2] column containing Porapak Q (90 cm×3.2 mm, 8/100 mesh), a

---

[2]Certain commercial materials are identified here in order to adequately specify the experimental procedure. In no case does this identification imply recommendation or endorsement by the National Bureau of Standards, nor does it imply that the material is necessarily the best available for the purpose.

232

membrane separator, and a quadrupole mass analyzer. Gases which were separated in time by the column passed through the membrane and were ionized by a 70-eV electron beam. The mass spectrometer was programmed to sample repetitively a sequence of selected ions characteristic of the various molecular species observed. Examples of single-ion chromatograms obtained by this procedure are shown in figures 3 and 4.

Table 2 indicates the ions monitored (mass-to-charge ratios, m/e), approximate column retention times, and corresponding boiling points at 100 kPa pressure for some of the species observed. The order of elution correlates with boiling points as expected and is like that previously reported for similar columns [9,14,15]. Retention time values varied somewhat depending on column temperature and carrier-gas flow rate. For most measurements the helium carrier-gas flow rate was 32 ml/min at a column temperature of 24 °C. Some mea-
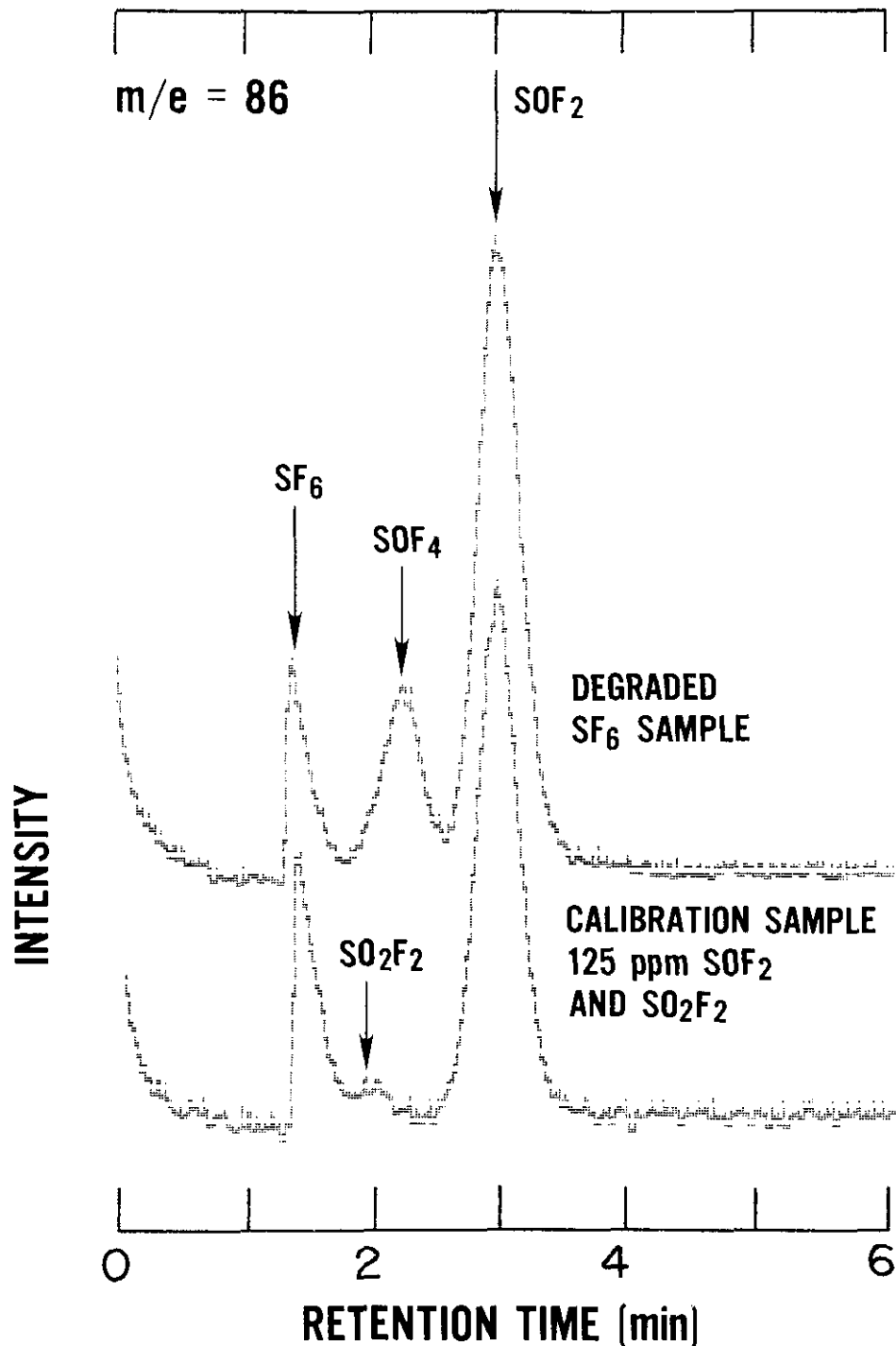
Figure 3–Typical single-ion chromatograms for $m/e = 86$ showing features associated with SF_6, SOF_2, SOF_4, and SO_2F_2 from decomposed SF_6 and from a calibration sample containing known amounts of SOF_2 and SO_2F_2 in SF_6. The gas sample injection was made at $t \simeq 1$ min.

233

m/e = 83   SO₂F₂

SOF₄

DEGRADED SF₆ SAMPLE

CALIBRATION SAMPLE
125 ppm SO₂F₂ AND
SOF₂ IN SF₆

INTENSITY

RETENTION TIME (min)
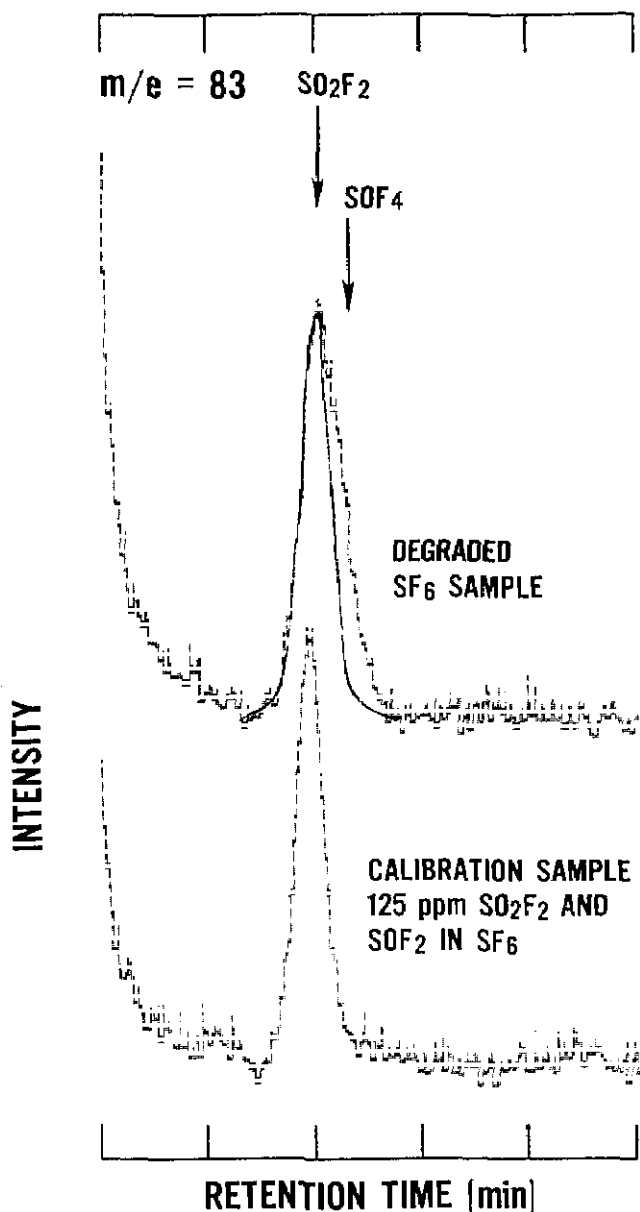
Figure 4—Typical single-ion chromatograms for $m/e = 83$ showing broadening of the SO_2F_2 peak due to SOF_4 in the sample of decomposed SF_6. The solid line represents a fit to the data of a curve which has a shape determined from calibration samples containing only SO_2F_2 and SOF_2. The area under the solid curve is then compared with that from calibration data to determine SO_2F_2 concentration.

surements were made at temperatures as high as 50 °C with a corresponding flow rate of about 18 ml/min.

The ions selected for monitoring were those that corresponded to the best signal-to-noise ratios. For SOF_2, the $m/e = 86$ data gave slightly better signal than $m/e = 67$, and for SO_2F_2, $m/e = 83$ gave the best results. However, analyses performed using both ions indicated for these gases gave results which were in satisfactory agreement. For SOF_4, only the $m/e = 86$ ion (SOF_2^+)

Table 2. Mass-to-charge ratios (m/e) of ions observed, approximate range of column retention times (at 24 °C and 32 ml/min He flow rate), and boiling points (at 100 kPa pressure) for various gaseous species observed.

Gas	Observed m/e	Retention Time (min)	Boiling Points (°C)
O_2	16	~0.2	−183.0
SF_3	19	0.35−0.48	−63.8
SO_2F_2	102,83	0.8−1.3	−55.4
SOF_4	86	1.0−1.6	−49.0
SOF_2	86,67	1.6−2.4	−43.8
H_2O	18,16	3.1−5.0	100.0
SO_2	64	8.2−8.7	−10.1

data could be used because of an excessively high background at $m/e = 105$ (SOF_4^+), and because of the method for quantitative analysis which, as described below, required a direct comparison with SOF_2 also appearing at $m/e = 86$.

In performing the gas analysis, samples of 0.8 ml volume were periodically (once every 1 to 2 h) extracted from the cell with a gas tight syringe and injected into the GC/MS. During the sampling period, about 4 min, the discharge was turned off. To assess the extent to which the equilibrium conditions in the cell were controlled by the discharge or influenced by relatively slow reactions in the bulk of the gas, the discharge was occasionally extinguished for long periods of up to 20 h. The gas was analyzed at the beginning and end of these periods.

3.3 GC/MS calibration

Quantitative analysis for the species SOF_2, SO_2F_2, SO_2, OCS, and CO_2, was accomplished by making direct comparisons of the GC/MS responses for unknown and reference gas samples as indicated by examples shown in figures 3 and 4. The absolute quantities in moles c were computed from the reference quantities c_r using $c = c_r(h_x/h_r)$, where h_x and h_r are respectively the responses for the unknown and reference samples corresponding to either normalized areas or peak heights of appropriate features in the chromatograms. All responses were normalized to the total SF_6 concentration, as indicated by the intensity S_{19} of the $m/e = 19$ (F^+) feature, such that $h_{x,r} = S_{x,r}/S_{19}$. Although the intensity S_{19} was found to be roughly proportional to the quantity of gas injected, care was taken to insure that the calibration and unknown samples contained nearly identical quantities of SF_6

The calibration samples were prepared in the discharge cell at the beginning and end of each experiment by injecting known quantities of SOF_2, etc., into "pure" SF_6. A secondary reference prepared in a separate cell

234

was also sometimes used during discharge operation. Calibration samples prepared in the discharge cell usually agreed satisfactorily with the secondary reference. Nevertheless, averages of several calibrations made at the end of each experiment from references prepared in the discharge cell were used to calculate the absolute quantities reported here. This choice eliminated errors associated with determination of discharge-to-reference cell volume ratios, and ensured highest accuracy for the highest unknown sample concentrations which, as discussed below, were given the greatest weight in making fits to the data to determine limiting constant production rates. The calibrations performed at the beginning and during the experiments were used to estimate uncertainties.

In many cases calibrations were performed over a range of c_r values from 10 to 85 μmoles. Because the response of the instrument was linear over the range of interest (see fig. 5), it was usually sufficient to use a single, relatively high value of c_r for these measurements.

Care had to be taken in determining S_x or S_r, to avoid errors due to peak interference, which was especially important in the case of SO_2F_2 as seen in figure 4. When SOF_4 was present, the SO_2F^+ peak at $m/e = 83$ was broadened due to conversion of SOF_4 into SO_2F_2 within the column or membrane by hydrolysis [43],

$$SOF_4 + H_2O \rightarrow SO_2F_2 + 2HF. \qquad (5)$$
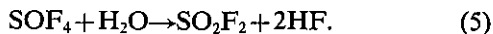
An investigation of the influence of SOF_4 on the SO_2F_2 feature revealed that it affected only the area to the right of the peak. To correct for SOF_4 interference the SO_2F_2 data were analyzed by calculating, after background subtraction, the area under a curve fit to the peak and left side with a shape which was defined by a fit to SO_2F_2 data ($m/e = 83$) from a reference sample not containing SOF_4. This is indicated by the solid curve in figure 4. Generally, the conditions were uniform and stable enough that the peak shapes did not change appreciably during the course of a given experiment. Thus for the relatively broad oxyfluoride peaks, it was usually sufficient to consider only peak heights in the determination of either S_x or S_r.
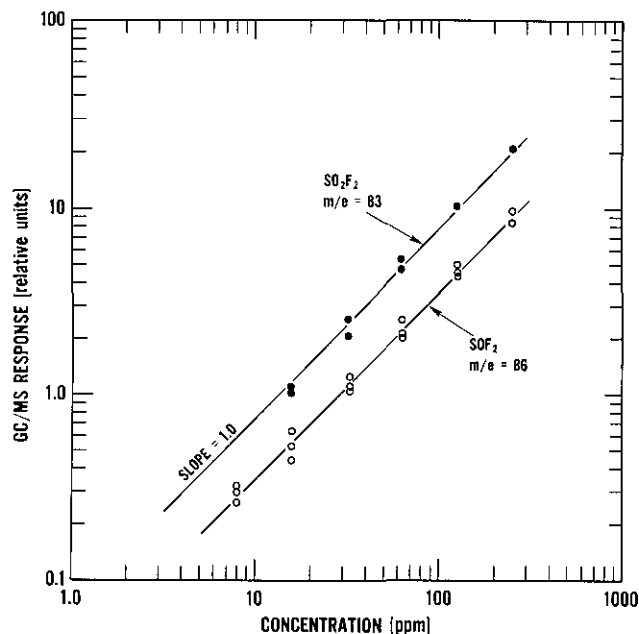
The analysis of SOF_4 data was complicated by difficulties encountered in preparing and maintaining reliable reference sample for this gas. In earlier work, [37,38] quantitative data for SOF_4 were not reported. Recently SOF_4 was prepared by the method of DesMarteau [44] from direct reaction of SOF_2 with F_2 in a pressurized vessel. In a few cases, direct calibrations for SOF_4 were performed as described for the other oxyfluorides. However, for most of the results given here, the SOF_4 data were put on an absolute scale by making a direct comparison with measured SOF_2 concentrations using data at $m/e = 86$.

From measurements made using many different reference samples containing different proportions of SOF_2 and SOF_4, the relative response r of the instrument to these species at $m/e = 86$ was determined, where

$$r = ([SOF_4]_r/[SOF_2]_r)(h_r(SOF_2)/h_r(SOF_4)). \qquad (6)$$

The unknown concentrations $[SOF_4]_x$ were then computed from the SOF_2 concentrations using

$$[SOF_4]_x = r\frac{h_x(SOF_4)}{h_x(SOF_2)}[SOF_2]_x. \qquad (7)$$

Examples of data from which SOF_4 concentrations were derived are shown in figure 6.

Either absolute of relative H_2O concentrations were measured in the gas for all cases. For the absolute measurements, the GC/MS calibration was performed using a previously calibrated, thin-film aluminum oxide hygrometer [45] inserted into the discharge cell containing SF_6. The responses of the GC/MS to water vapor at $m/e = 18$ and $m/e = 16$ were compared to simultaneous readings from the hygrometer after sufficient time elapsed, usually more than 10 h, for the system to reach equilibrium. Because of the slow response time of the hygrometer and its susceptibility to damage from corrosive discharge by-products, it could not be used directly to monitor H_2O during discharge activity.

Figure 5–Calibration curves for SO_2F_2 and SOF_2 showing relative GC/MS response versus concentration.

235
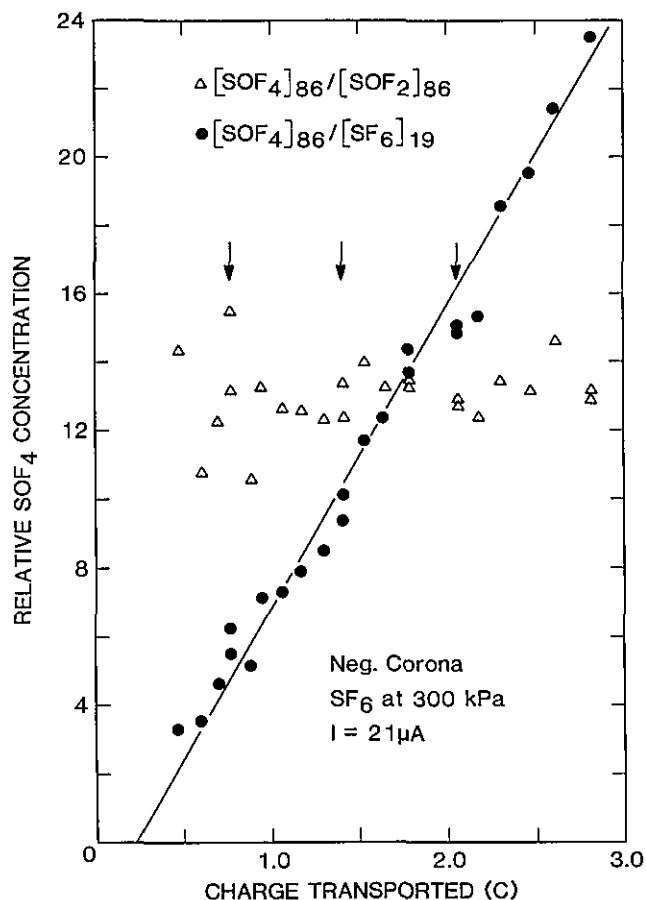
Figure 6–Relative normalized GC/MS response to SOF₄ and the ratios of SOF₄ to SOF₂ responses at $m/e = 86$ versus net charge transported for 300 kPa SF₆ decomposed in negative corona at 21 μA. The arrows indicate times when the discharge was off for extended periods.

4. Results

4.1 Products Observed

The SF₆ gas was always analyzed after introduction into the cell and prior to turning on the discharge. The most common initial contaminants observed were varying trace amounts of CF₄, H₂O, and air. Although the discharge chamber was evacuated to 1.3×10^{-5} Pa ($\sim 1 \times 10^{-7}$ Torr) before introducing the gas, it was not baked. Therefore, if left undisturbed, the water vapor concentration would build up slowly to an equilibrium level. In most cases it would rise from initial levels of less than 10 ppm by volume to an equilibrium level between about 150 and 300 ppm by volume determined by the ambient temperature, initial cleanliness of surfaces, etc. The initial H₂O concentration at the start of the discharge was thus determined by the time that the gas had been left undisturbed in the cell. Once the discharge was initiated, the concentration of H₂O was al-

ways observed to increase more rapidly than normal, presumably because of desorption from surfaces heated by the discharge [37]. However, the maximum H₂O concentration never significantly exceeded that associated with equilibrium under normal, undisturbed conditions. In later stages of discharge operation, a slow decrease in H₂O content was usually observed, which, as discussed later, was undoubtedly indicative of the role played by gas-phase H₂O in the discharge chemistry.

The O₂ concentration was observed to gradually increase during operation of the discharge. In "pure" SF₆, its concentration was always too small to measure accurately by the present method. The increase in O₂ content during these experiments could be accounted for by release from electrode materials during the discharge and from introduction of low levels of air contamination during gas sampling. To assess its role in oxyfluoride production, a few measurements were made with controlled levels of O₂ between 1 and 10% content by volume.

Of the observable species generated in the discharge, the oxyfluorides SOF₂, SO₂F₂, and SOF₄ were produced in greatest abundance. Other highly reactive species such as HF and F₂ possibly formed in conjunction with the oxyfluorides at comparable rates could not be observed by the GC/MS method used. One could argue that on the time scales considered here these are not really stable since they can be expected to react rapidly with other materials in the discharge chamber.

Of the remaining species which could be observed in the gas only SO₂, OCS, CO₂, and previously mentioned O₂, showed clear evidence of build-up during the discharge. The formation rates of all these species were considerably lower than those for the oxyfluorides. Slow production of CO and CF₄ may also have occurred in some cases, but reliable data on these could not be obtained.

Besides the gaseous products which were observed, clear evidence of S⁻ ion deposition appeared on the anode for negative corona currents in excess of about 60 μA. Introduction of O₂ caused sulfur deposits to appear at lower currents. Changes in electrode surfaces were evident in all experiments, but no attempt was made to characterize these changes except to note that the surface of the point electrode always exhibited more deposits and pitting for positive discharges than for negative discharges of comparable current.

4.2 Quantitative Analysis

The minimum detectable quantity for all the species observed was about 1.0 μmole. The experiments were typically terminated before the quantity of any oxy-

236

fluoride within the discharge chamber exceeded about 100 μmoles.

The major sources of uncertainty in the quantitative analysis were due to drifts in the GC/MS response and uncertainties in the reference samples. The dominant short-term drift associated with heating of the mass spectrometer ion source by the electron gun filament could be largely overcome by heating the source prior to gas sample injection. Of more significance in determining overall uncertainty were long-term drifts associated, for example, with slow changes in mass spectrometer tuning, ion detection efficiency, and GC-column conditions. To reduce accidental errors associated with reference sample preparations, several calibrations were always performed with different reference samples.

The estimated uncertainties in measured absolute SOF_2 and SO_2F_2 concentrations are less than ±25%. The SOF_4 uncertainties are higher (±45%) because of the indirect method of determination and the required assumption that the relative GC/MS responses to SOF_2 and SOF_4 at $m/e = 86$ remained constant.

4.3 Production Rates

The production rates were derived from fits to the measured concentration data plotted versus either net energy dissipated or charge transported as shown in figures 7–13. The term "concentration" refers here to the absolute quantity of gas in moles which was produced in the discharge and which was assumed to be uniformly distributed within the cell volume. The production curves in most cases exhibit deviations from linearity which are most evident at the lowest values of u or Q. Best fits to the data over the entire ranges were found to be of the forms:

$$c(u)=c_0'+A'u^{1+\epsilon'}, \quad c(Q)=c_0+A\,Q^{1+\epsilon}, \tag{8}$$

where c_0, c_0', A, A', ϵ, and ϵ' are fitting parameters. The first pair allows for a small, usually undetectable initial concentrations, and the last pair represents a measure of deviations from linearity. Examples of values obtained for these parameters are tabulated and discussed in the Appendix.
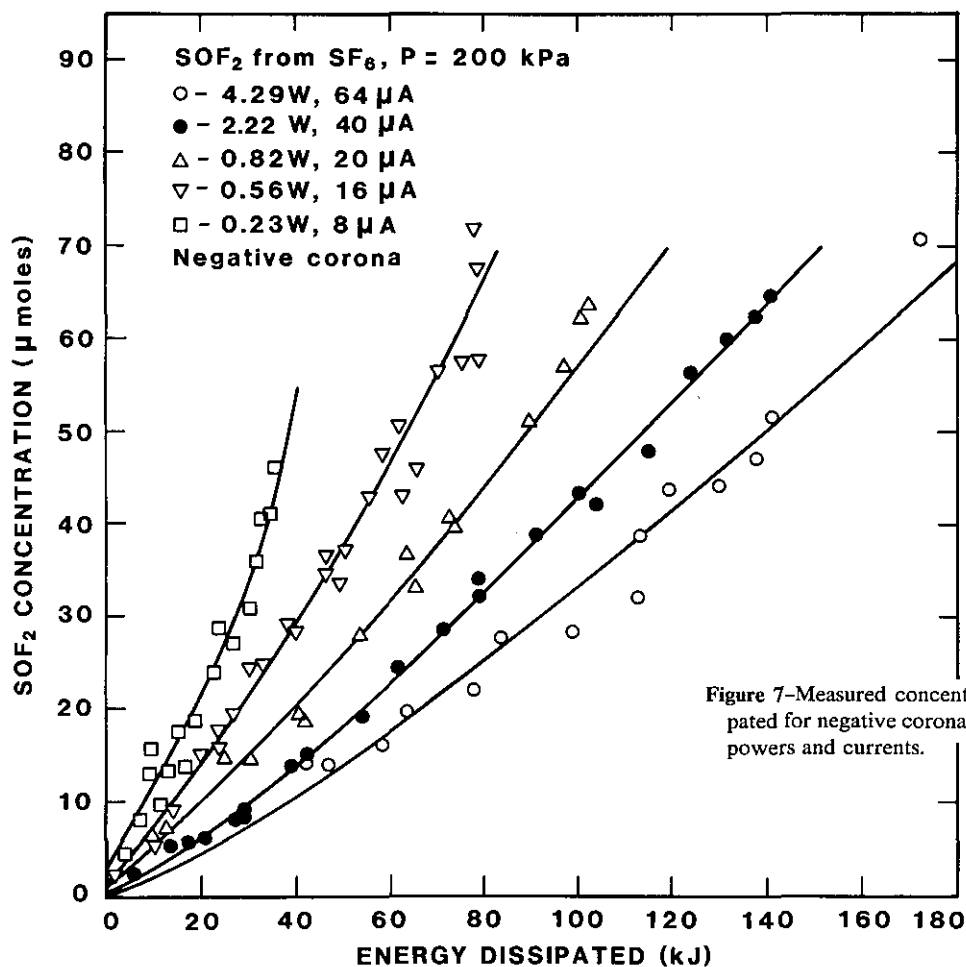
Figure 7–Measured concentrations of SOF_2 versus net energy dissipated for negative corona in 200 kPa SF_6 at the indicated discharge powers and currents.

237
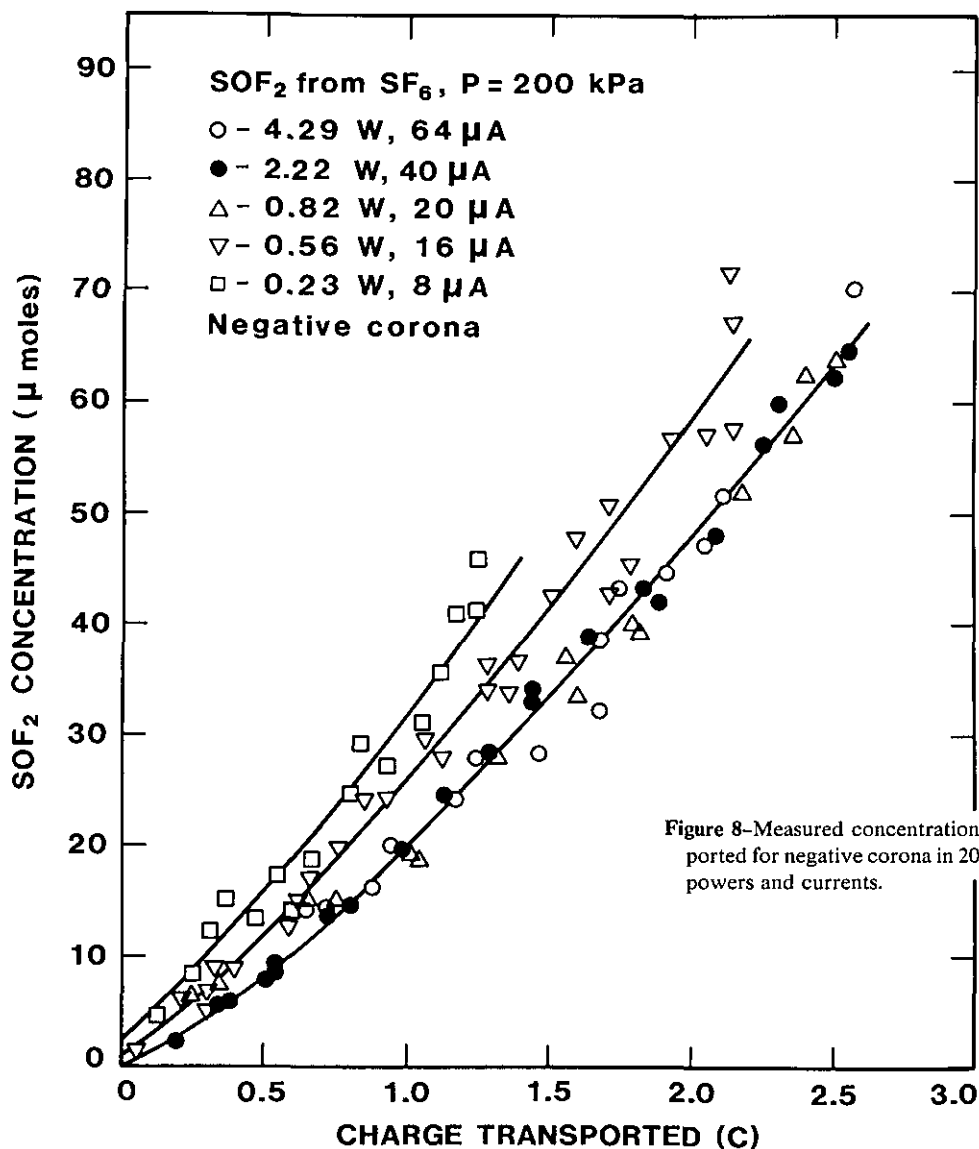
Figure 8–Measured concentrations of SOF₂ versus net charge transported for negative corona in 200 kPa SF₆ at the indicated discharge powers and currents.

It was found for SOF_2 and SO_2F_2 production that $1 > \epsilon > 0$ in all cases, indicating rates that tend to increase with time. However, with few exceptions, the rates appeared to approach constant values corresponding to straight line fits to the data at the higher u or Q values as shown in figures 11–13. In the case of SOF_4, again $1 > \epsilon > 0$ was found for positive-polarity data, but $\epsilon \approx 0$ gave the best fits for most negative-polarity data (see fig. 6).

The initial increase in the production rates is not understood but could be associated with absorption of the product gases on the walls and thus with times required to establish equilibrium within the discharge vessel. This effect might also be related to the rates of gas-phase reactions that depend on availability of oxygen containing contaminants required for oxyfluoride formation such as H_2O and O_2 which often initially increased after onset of the discharge. However, measurements made

with differing initial concentrations of these gases at low levels showed no well-defined influence on the degree of nonlinearity. As will be discussed later, a significant contribution from secondary reactions is another factor which could introduce nonlinearities. "Secondary reactions" are those such as reaction (5), whereby the production of a given species is affected by the concentrations of other species generated in the discharge. Attempts to interpret deviations from linearity were complicated by the observation that the results from the early stages of discharge activity were generally less reproducible than the later, higher concentration data that give the limiting constant rates corresponding to the linear fits shown in figures 11–13.

Instantaneous production rates for particular values of u and Q can be computed from fits of the forms given by eq (8) as previously reported [38] (see the Appendix). The limiting constant rates, however, appear to be more

238
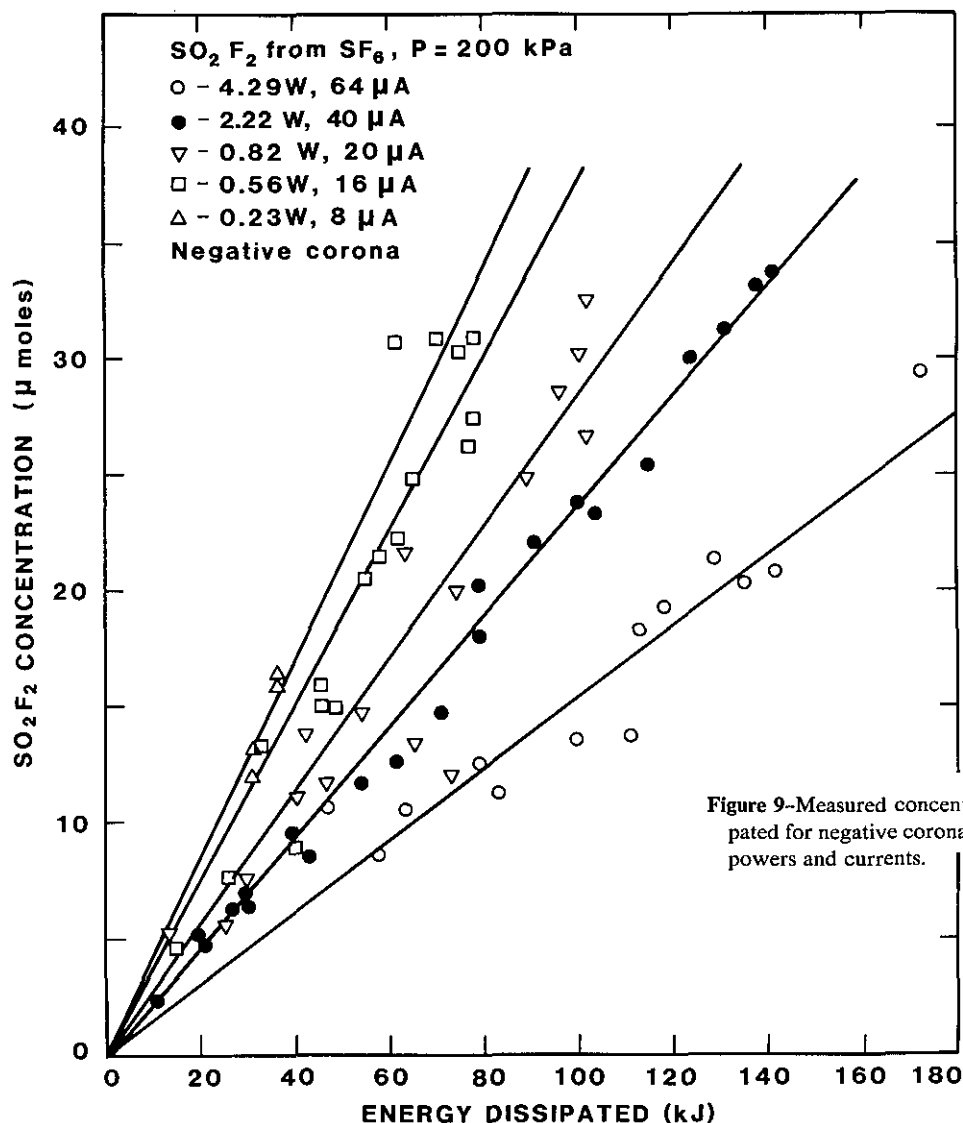
Figure 9--Measured concentrations of SO_2F_2 versus net energy dissipated for negative corona in 200 kPa SF_6 at the indicated discharge powers and currents.

useful in describing trends as functions of gas or discharge conditions. A precise definition of these rates and their relationship to the instantaneous rates from eq (8) are given in the Appendix.

Results for the limiting constant production rates of SOF_2, SO_2F_2, and SOF_4 are given in tables 3-5. Both r_u and r_q are listed as functions of discharge conditions (polarity, current, and power) and gas pressure. Gas pressures range from 114 kPa (~ 1.1 atm) to 300 kPa (~ 3 atm). Discharge currents from 1.5 μA to 64 μA with corresponding power dissipations from 0.054 W to 4.3 W are included.

Production rates were estimated in some cases for observable minor species, namely SO_2, OCS, and CO_2 as indicated in table 6. The rates for these are seen to be an order of magnitude or more smaller that those for the predominant oxyfluorides. Data for SO_2 are also shown in figure 13.

Although the results showed indications of gas-phase H_2O consumption, particularly in the later stages of discharge activity (see figs. 11-13), no attempt was made to determine the rates of consumption. The discharge appeared to suppress the equilibrium level of H_2O in the cell, and there was evidence that the degree of suppression increased with increasing current and therefore increasing oxyfluoride production (compare figs. 12 and 13). It was found in more recent studies [46] with corona in SF_6/O_2 mixtures that the CO_2 production is nonlinear and depends significantly on O_2 content and availability of carbon from the electrode surface. The same may apply to OCS, although this could not be ascertained from the data obtained.

Based on the previously noted dominant sources of error in quantitative analysis and the uncertainties in fitting the data, the limiting rate values given in tables 3 and 4 for SOF_2 and SO_2F_2 have been assigned a max-

239

Table 3. Limiting constant values for SOF₂ production rates.

Polarity	Discharge Power (W)	Discharge Current (μA)	Gas Pressure (kPa)	Production Rates (nmoles/J)	Production Rates (μmoles/C)
Pos.	0.804	20.0	116	1.28	49.5
	0.054	1.5	200	5.20	181
	0.335	8.0	200	4.69	195
	0.777	16.0	200	3.80	180
	0.198	4.0	300	4.06	187
	0.430	8.0	300	3.09	178
	0.945	16.0	300	2.64	172
Neg.	0.898	25.0	144	1.21	45.0
	0.230	8.0	200	1.52	35.2
	0.586	16.0	200	0.93	34.7
	0.821	20.0	200	0.68	34.1
	2.225	40.0	200	0.54	32.4
	4.290	64.0	200	0.44	33.7
	0.764	16.0	300	0.73	31.2
	1.140	21.0	300	0.41	23.9
	1.820	30.0	300	0.33	22.3

Table 4. Limiting constant values for SO₂F₂ production rates.

Polarity	Discharge Power (W)	Discharge Current (μA)	Gas Pressure (kPa)	Production Rates (nmoles/J)	Production Rates (μmoles/C)
Pos.	0.804	20.0	116	1.83	69.7
	0.054	1.5	200	4.51	151
	0.154	4.0	200	4.07	158
	0.335	8.0	200	3.27	147
	0.777	16.0	200	2.10	109
	0.198	4.0	300	2.32	119
	0.430	8.0	300	2.03	113
	0.945	16.0	300	1.29	111
Neg.	0.898	25.0	144	0.52	18.0
	0.230	8.0	200	0.62	16.0
	0.586	16.0	200	0.47	16.9
	0.821	20.0	200	0.36	14.8
	2.215	40.0	200	0.25	13.9
	4.290	64.0	200	0.16	12.6
	0.764	16.0	300	0.38	17.9
	1.140	21.0	300	0.29	16.9

SO₂F₂ from SF₆ , P = 200 kPa
○ − 4.29W, 64 μA
● − 2.22 W, 40 μA
▽ − 0.82W, 20 μA
□ − 0.56W, 16 μA
△ − 0.23W, 8 μA
Negative corona
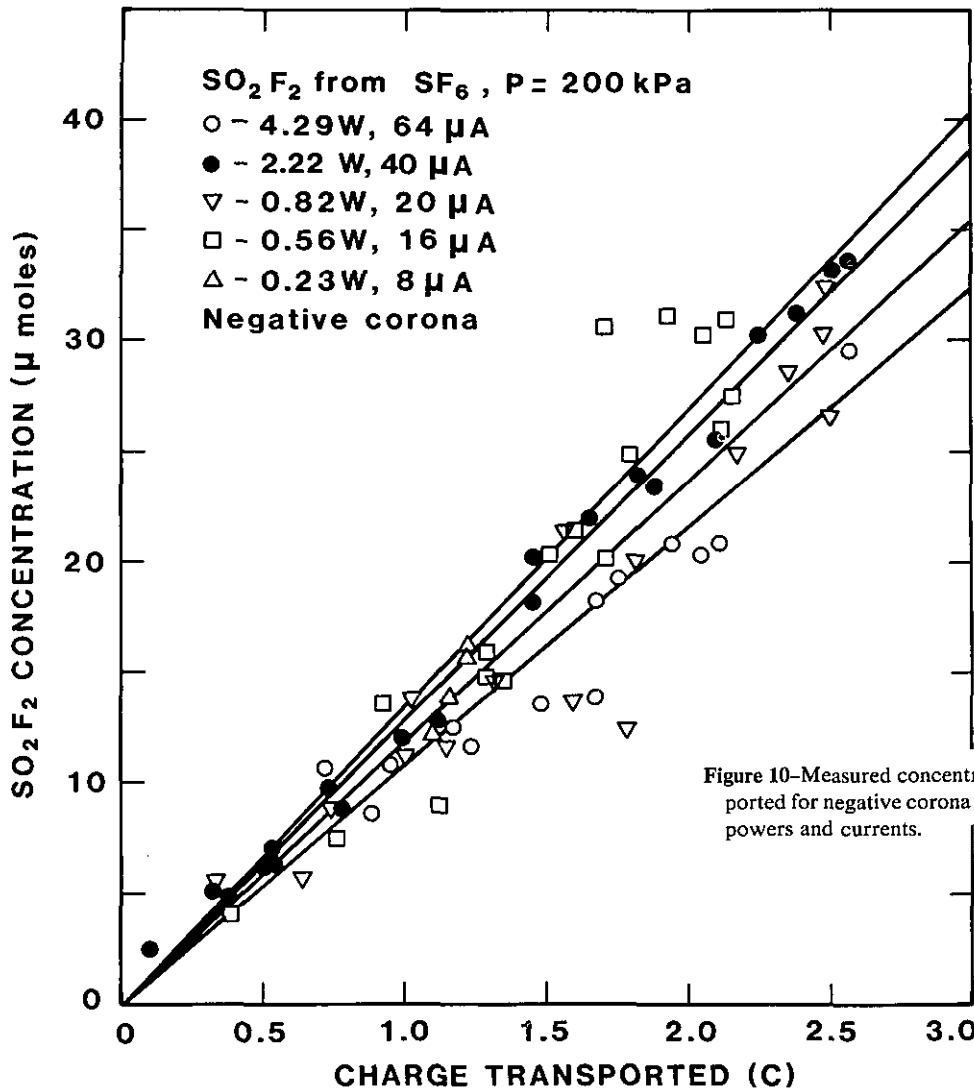
Figure 10–Measured concentrations of SO₂F₂ versus net charge transported for negative corona in 200 kPa SF₆ at the indicated discharge powers and currents.
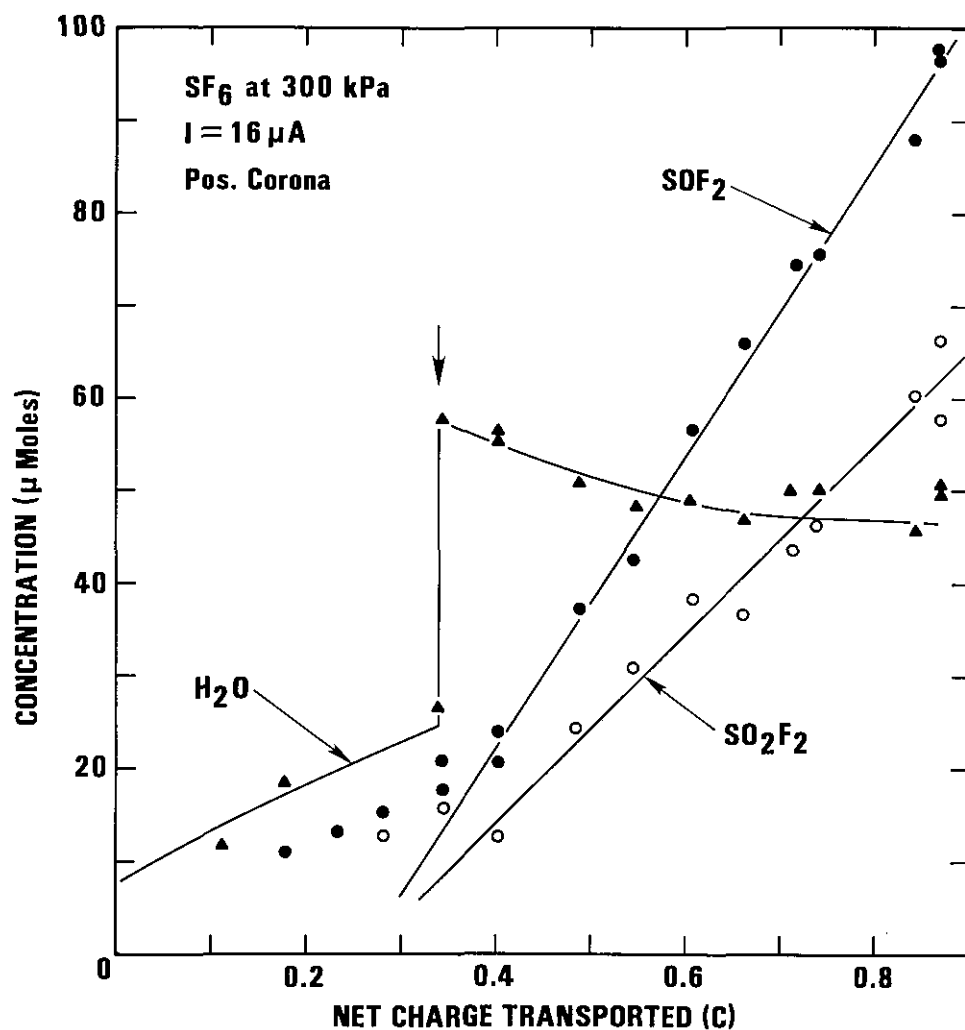
Figure 11-Measured absolute concentrations of SOF_2 and SO_2F_2 and relative concentrations of H_2O versus net charge transported for positive corona in 300 kPa SF_6 at 16 μA. The arrow indicates a time when the discharge was off for an extended period.

Table 5. Limiting constant values for SOF_4 production rates.

Polarity	Discharge Power (W)	Discharge Current (μA)	Gas Pressure (kPa)	Production Rates (nmoles/J)	Production Rates ($\mu moles/C$)
Pos.	0.804	20.0	116	7.02	290
	0.054	1.5	200	7.04	260
	0.335	8.0	200	8.60	373
	0.777	16.0	200	8.45	418
	0.198	4.0	300	5.79	292
	0.430	8.0	300	5.92	343
	0.945	16.0	300	7.08	431
Neg.	0.898	25.0	144	0.85	30.1
	0.230	8.0	200	0.92	23.8
	0.586	16.0	200	0.97	34.6
	0.821	20.0	200	1.05	41.5
	2.215	40.0	200	0.90	49.7
	4.290	64.0	200	0.94	63.6
	0.764	16.0	300	0.44	20.6
	1.140	21.0	300	0.39	21.0

Table 6. Estimated production rates for minor species from negative corona in SF_6.

Species	Discharge Current (μA)	Pressure (kPa)	Production Rates (nmoles/J)	Production Rates ($\mu moles/C$)
SO_2	25	114	0.008	0.3
SO_2	40	200	0.002	0.1
OCS	40	200	1.3×10^{-5}	7.2×10^{-3}
CO_2	40	200	0.035	2.0

imum uncertainty of $\pm 35\%$. The rates for SOF_2 typically have less uncertainty than those for SO_2F_2, and results from positive corona have higher uncertainty than those from negative corona. The latter trend is due to the greater fluctuations in the discharge current (see fig. 2). The uncertainties for SOF_4 are higher but are estimated to be always less than $\pm 57\%$. The rates given in table 6 for the minor products are only estimates since a reasonable error assessment was impossible.

CONCENTRATION (μ Moles)

SF$_6$ at 200 kPa

I = 40 μA

Neg. Corona

SOF$_2$

SO$_2$F$_2$

H$_2$O

NET CHARGE TRANSPORTED (C)
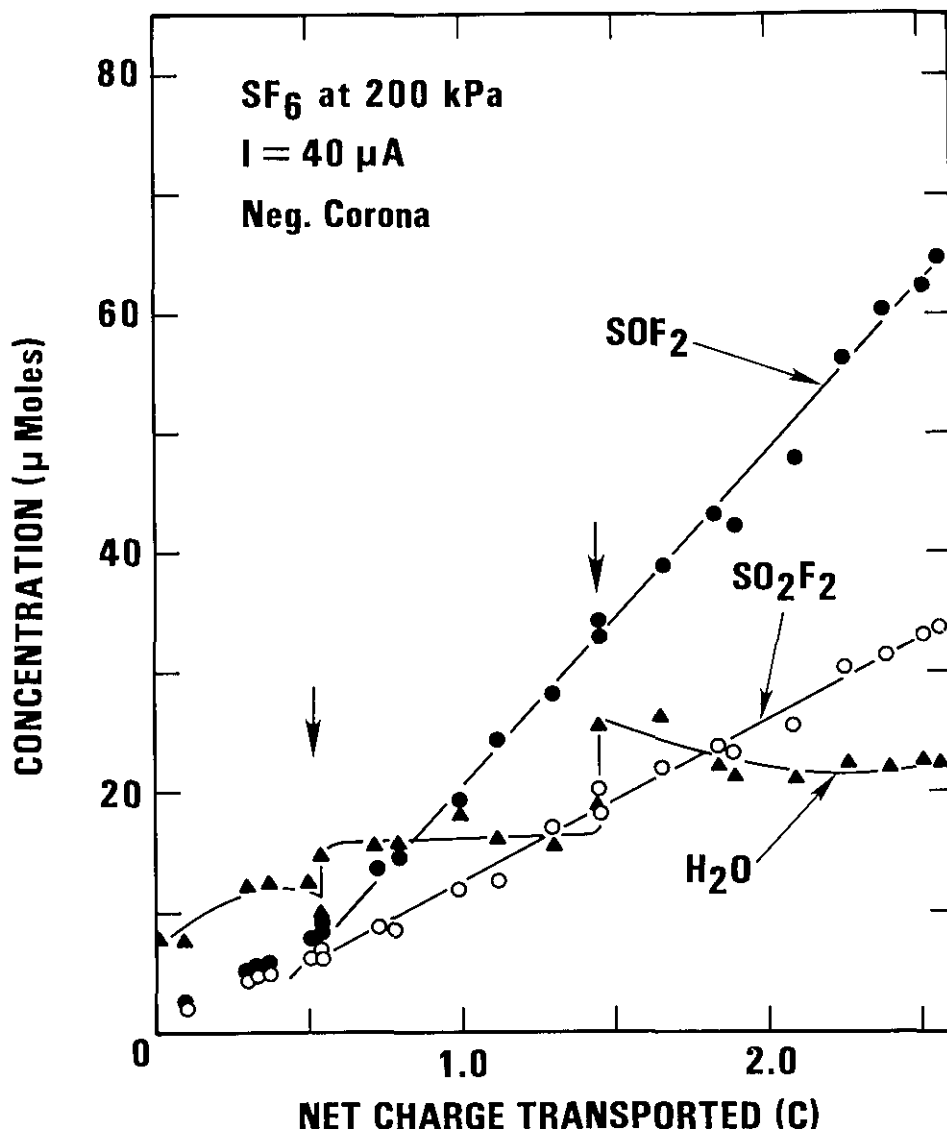
Figure 12–Measured absolute concentrations of SOF$_2$, SO$_2$F$_2$, and H$_2$O versus net charge transported for negative corona in 200 kPa SF$_6$ at 40 μA. The arrows indicate times when the discharge was off for extended periods.

Important observations from the data in tables 3–5 include:

1) The production rates for SOF$_2$, SO$_2$F$_2$, and SOF$_4$ are of comparable magnitude to within roughly a factor of 3. For most cases, particularly at the higher pressures and power levels, the order of production rates is $r_q(SOF_4) > r_q(SOF_2) > r_q(SO_2F_2)$.

2) Oxyfluoride production does not change dramatically with pressure. One exception is the large relative drop in the SOF$_2$ and SO$_2$F$_2$ rates compared to SOF$_4$ in going from 200 to 116 kPa for positive polarity.

3) Oxyfluoride production under most conditions increases by a factor of 5 or more in going from negative to positive polarities for discharges of comparable power levels.

4) The charge rates-of-production for SOF$_2$ and SO$_2$F$_2$ vary less with discharge level than the corresponding energy rates, whereas the opposite appears to be true for SOF$_4$ (see also figs. 14 and 15).

The trends noted for SOF$_2$ and SO$_2$F$_2$ from the fourth observation imply that the time rates-of-production for these are more nearly directly proportional to the current than the power, i.e., $dc/dt \propto i$. Because of the relatively large uncertainties, it can only be stated that the SOF$_4$ rates behave like $dc/dt \propto i^a$, with $1 < a < 2$. The results in figure 15 would in fact suggest that $dc/dt \propto p$ for this species.

The vertical arrows in figures 6 and 11–13 indicate times when the discharge was turned off for periods of 12 to 20 h. No significant changes in the oxyfluoride content occurred during these times, therefore indicating that reactions involving the oxyfluorides in the

242
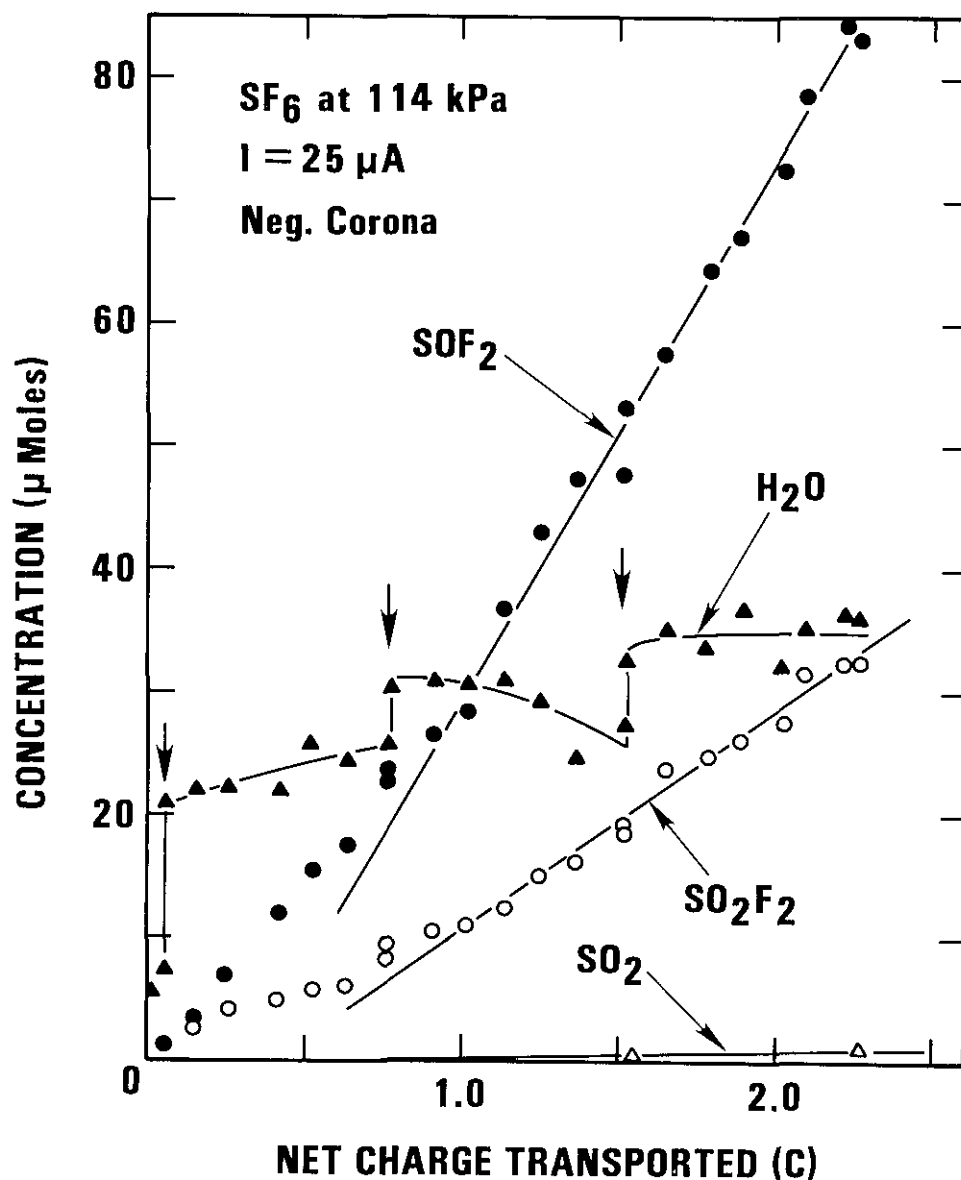
Figure 13-Measured absolute concentrations of SOF_2, SO_2F_2, SO_2, and H_2O versus net charge transported for negative corona in 114 kPa SF_6 at 25 μA. The arrows indicate times when the discharge was off for extended periods.

bulk of the gas outside the discharge region were too slow to observe. The H_2O concentrations on the other hand exhibited increases during times when the discharge was off (see figures 11–13), consistent with the previously noted evidence that chemical processes associated with the discharge consume water vapor and suppress its equilibrium level in the gas.

4.4 SF_6/O_2 Mixtures

Extensive studies of discharge-induced gas chemistry in SF_6/O_2 and SF_6/N_2 mixtures are currently underway and will be reported later [46]. Because of the possible importance of gas-phase O_2 in oxyfluoride production, an assessment of its role could only be made by considering mixtures in which its content was increased significantly above the normally occurring trace levels over which there was no control. Results are shown in figures 16–18 for SOF_2, SO_2F_2, and SOF_4 production in mixtures containing 1 to 10% O_2 in SF_6 compared with "pure" SF_6 containing the normal trace amounts of O_2. The measurements for all these mixtures were performed at the same indicated total gas pressure and discharge current. The error bars correspond to estimated uncertainties in measured absolute concentrations.

These results show that to within the measurement uncertainties the addition of 1% O_2 has virtually no influence on the production of the oxyfluorides. However, at higher O_2 content, the total oxyfluoride yield actually drops, and the drop is most evident for SOF_2 (see fig. 16).

243
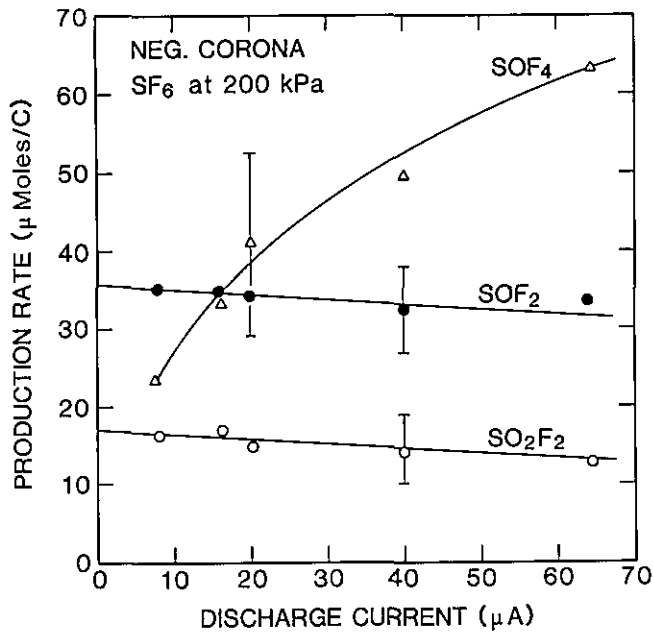
Figure 14–Measured charge rates of production for SOF₄, SOF₂, and SO₂F₂ versus discharge current for negative corona in 200 kPa SF₆.
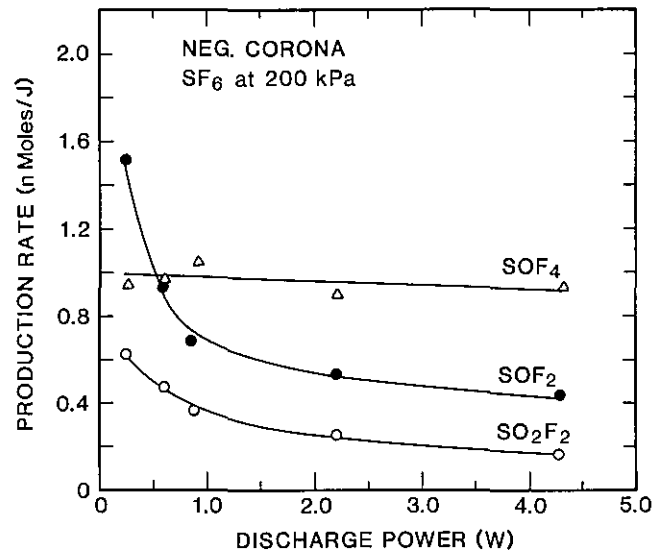
Figure 15–Measured energy rates of production for SOF_4, SOF_2, and SO_2F_2 versus discharge power for negative corona in 200 kPa SF_6.
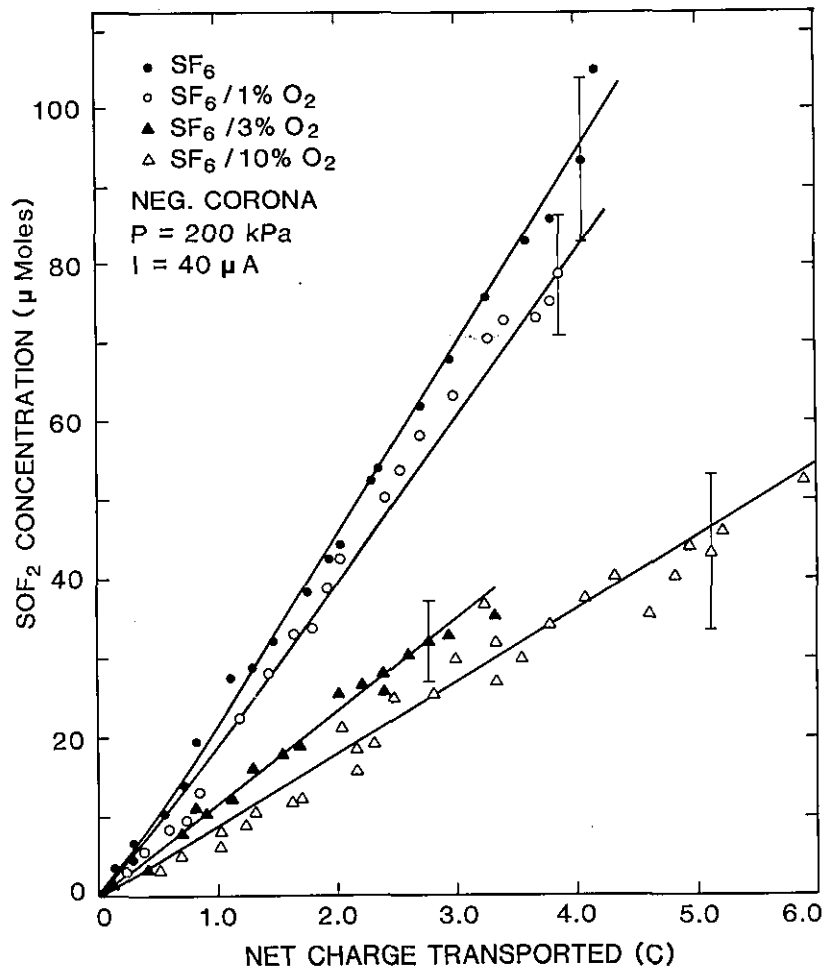
Figure 16–Measured absolute SOF_2 concentrations versus net charge transported for 40 µA negative corona in SF_6/O_2 mixtures containing the indicated percent-by-volume concentrations of O_2. The "pure" SF_6 contained trace levels of O_2 which could not be accurately determined.

244
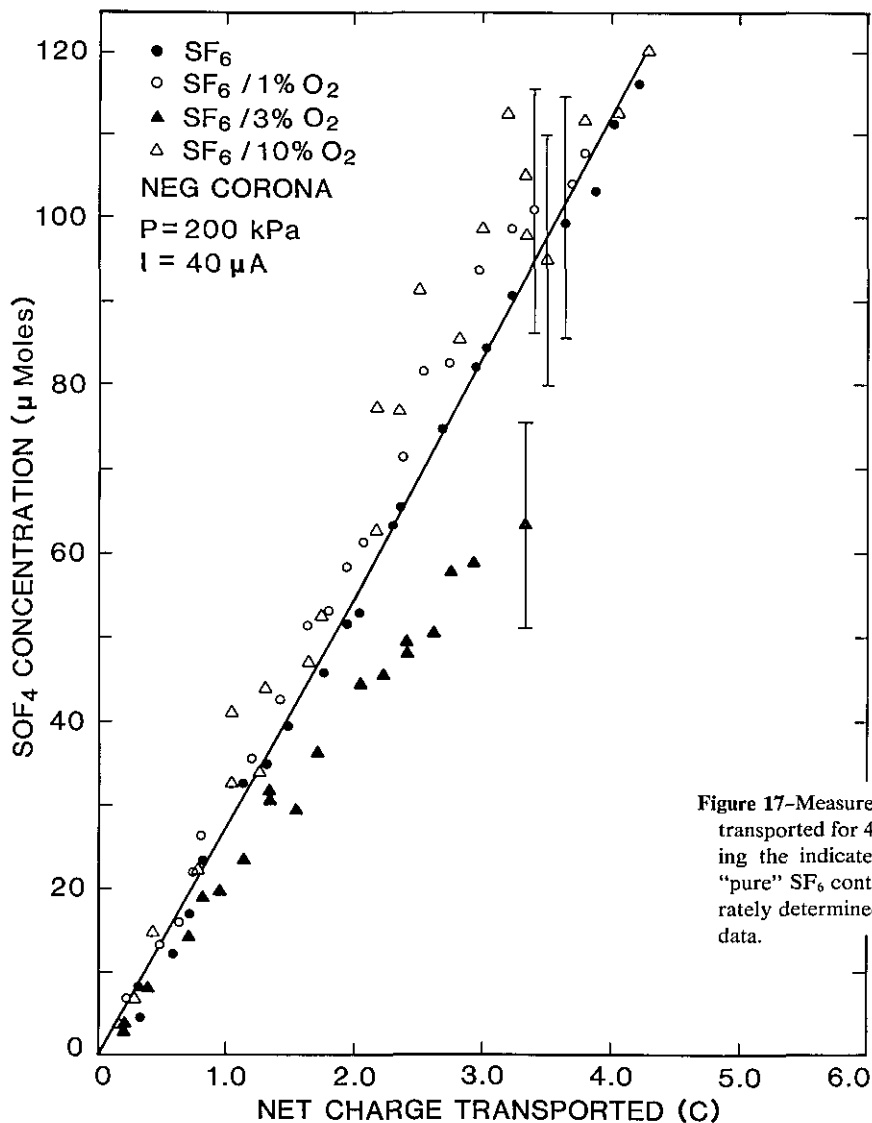
Figure 17–Measured absolute SOF_4 concentrations versus net charge transported for 40 μA negative corona in SF_6/O_2 mixtures containing the indicated percent-by-volume concentrations of O_2. The "pure" SF_6 contained trace levels of O_2 which could not be accurately determined. The solid line represents a fit to the "pure" SF_6 data.

5. Discussion

5.1 Comparisons With Previous Observations

The oxyfluoride production rates found here are comparable in magnitude to many of those previously reported in other types of SF_6 electric discharges (see table 1). However, any comparisons with other results is of questionable significance since all previous measurements were performed under dissimilar conditions. The measurements by Chu et al. [18], which are most nearly like those of the present experiments, were perormed with corona generated by 60-Hz ac voltage applied to aluminum electrodes in SF_6 at a pressure of about 155 kPa. The corona evidently occurred near the peaks of each half-cycle and was mainly characterized by pulses with an average magnitude of 10^3 pC and a repetition rate of 2 kHz. From the information provided, the total $SOF_2+SO_2F_2$ production rate from this

measurement is estimated to lie between 620 and 1400 μmoles/C. The conditions most like this in the present work would correspond to the positive discharge at 1.5 μA which yielded a net rate for $SOF_2+SO_2F_2+SOF_4$ production of 592 μmoles/C.

Although the present result is close to that of Chu et al., it is disturbing that they do not observe SOF_4. It is conceivable that this can be explained by a conversion of SOF_4 to SO_2F_2 via reaction (eq (5)) in the gas sampling process. Other cases [14,24] where there was failure to see SOF_4 from corona or "weak-current" discharges in SF_6, even though SO_2F_2 was reported to be a predominant product, might also be accounted for by hydrolysis of SOF_4. There are documented cases [8–10,23] where SOF_4 was observed in low-current discharges and even appeared as the dominant product.

Boudene et al. [15], Sauers et al. [20,39], and Castonguay [22] all report total oxyfluoride energy rates-of-

245
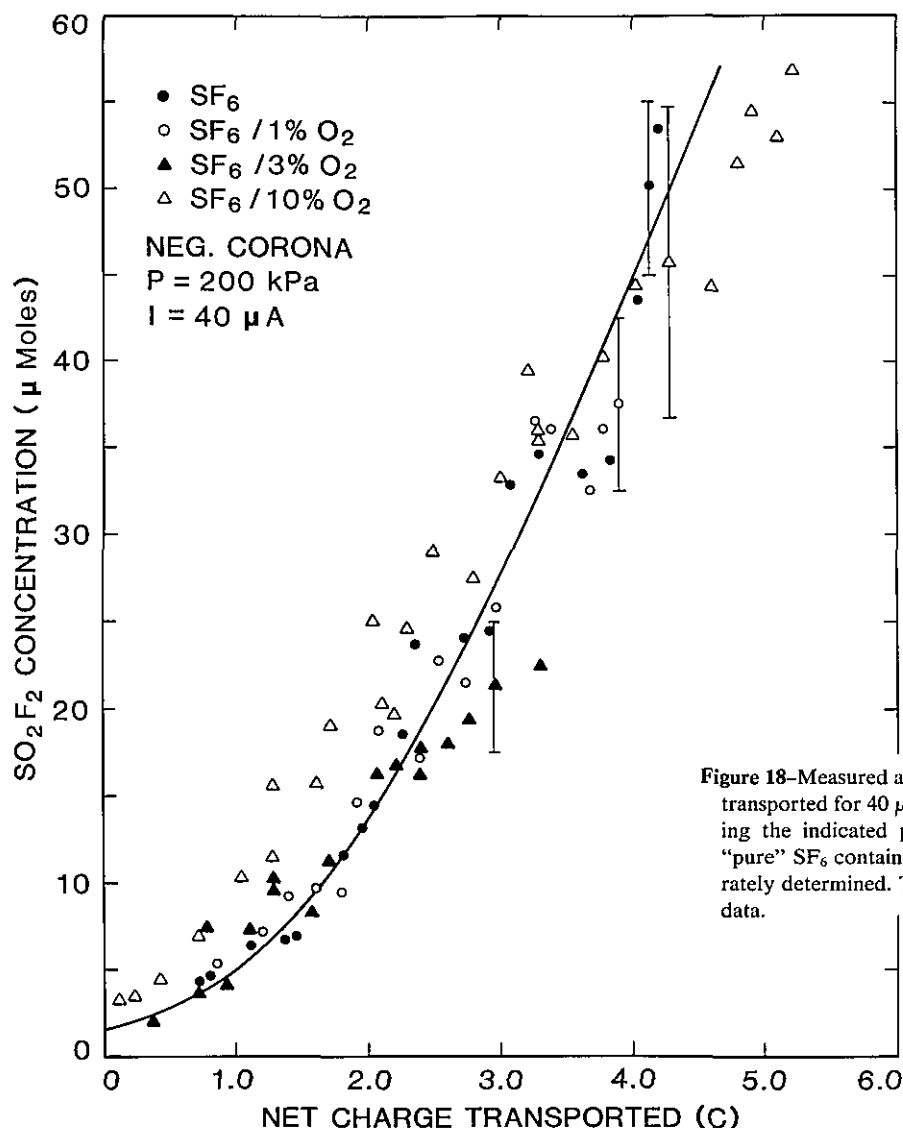
Figure 18-Measured absolute SO_2F_2 concentrations versus net charge transported for 40 μA negative corona in SF_6/O_2 mixtures containing the indicated percent-by-volume concentrations of O_2. The "pure" SF_6 contained trace levels of O_2 which could not be accurately determined. The solid line represents a fit to the "pure" SF_6 data.

production in SF_6 arcs and sparks with stainless steel electrodes that are comparable in magnitude to some of the rates found here (see table 1). However, in these types of discharges, which generate predominantly SOF_2, metal vapors and thermal dissociation may play an important role because of the high levels of power dissipation. The present results are consistent with previous observations and arguments [14,16,19,24] that SO_2F_2 and SOF_4 should become more prevalent as by-products when the discharge power level is reduced.

Net time rates-of-production that are directly proportional to discharge current rather than power are shown in recent relative measurements by Ophel et al. [26] of the total hydrolyzable fluoride production from stainless steel point-plane corona in flowing SF_6 at 440 kPa. This behavior would be consistent only with the results found here for SOF_2 and SO_2F_2. Were SOF_4 to become

a major component among the hydrolyzable species detected, then the present results indicate that for a single point electrode, proportionality to current need not be expected.

5.2 Possible Mechanisms for Oxyfluoride Formation

It is useful as a guide to the interpretation of the results to consider some of the plausible sequences of reactions which could account for production of SOF_2, SO_2F_2, and SOF_4 in a corona discharge. It should be cautioned, however, that the chemical processes that can occur in an electrical discharge are undoubtedly of a complicated, multistep nature, and no attempt will be made to present an exhaustive listing of the multitude of reactions possible. Instead the discussion here will be limited to previously suggested processes that appear relevant to the interpretation of the present results.

246

A corona is a relatively weak plasma in which the electron temperature greatly exceeds the gas temperature and in which nonequilibrium conditions prevail [47]. It is therefore expected that the initial stage of SF_6 decomposition predominantly results from dissociation of molecules by electron collisions. At electric field-to-gas density ratios, E/N, close to the critical value where a growth in the net ionization of the gas becomes possible, the mean electron energies in an SF_6 discharge are theoretically estimated [48–50] to be between 5 and 10 eV. Thus from a consideration of the known ionization, attachment, and bond dissociation energies [51–56] of SF_6, the initial step in the decomposition is presumed to involve the energetically favorable electron impact dissociation processes leading to various ion and neutral fragments, e.g.,

$$e + SF_6 \rightarrow SF_x + (6-x)F, \ x \leqslant 5. \quad (9)$$
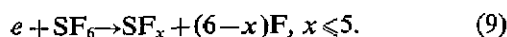
Multistep dissociation might also contribute, e.g., dissociation of the fragment such as $e + SF_4 \rightarrow SF_3 + F + e$. From energetic considerations, the greatest contribution will probably be from dissociation leading to the larger neutral fragments SF_x, $x = 3, 4, 5$. This presumption is supported by calculations by Masek et al. [57] of dissociative fragment production rates from electron swarms in SF_6 and SF_6/O_2 mixtures using numerical solutions of the Boltzmann equation. Moreover, the species SF_4 is reported to be the most stable and most abundant primary product from both thermal dissociation of SF_6 at moderate temperatures [60–61] and from relatively cool electric discharges [20,21,30].

It is known [8] that in the absence of reactive surfaces or gaseous contaminants, the products of SF_6 dissociation rapidly recombine through relatively fast processes such as proposed by Gonzalez and Schumacher [58] to explain the observed thermal conversion of $SF_4 + F_2$ into SF_6. The presence of oxygen, or oxygen containing species in the discharge region can interfere with the recombination process and give rise to the formation of oxyfluorides, free fluorine, and HF. Some of the energetically favorable bimolecular reactions that could lead directly to oxyfluoride formation include [62]:

$$SF_5 + OH \rightarrow SOF_4 + HF, \ \Delta H^\circ_{298} = -464 \ kJ/mol, \quad (10)$$

$$SF_5 + O \rightarrow SOF_4 + F, \ \Delta H^\circ_{298} = -327 \ kJ/mol, \quad (11)$$

$$SF_4 + O \rightarrow SOF_4, \ \Delta H^\circ_{298} = -549 \ kJ/mol, \quad (12)$$

$$SF_4 + O \rightarrow SOF_2 + 2F, \ \Delta H^\circ_{298} = -124 \ kJ/mol, \quad (13)$$

$$SF_3 + O \rightarrow SOF_2 + F, \ \Delta H^\circ_{298} = -213 \ kJ/mol, \quad (14)$$

$$SF_2 + O \rightarrow SOF_2, \ \Delta H^\circ_{298} = -496 \ kJ/mol, \quad (15)$$

$$SF_4 + OH \rightarrow SOF_2 + HF + F, \Delta H^\circ_{298} = -130 kJ/mol, \quad (16)$$

$$SF_3 + OH \rightarrow SOF_2 + HF, \ \Delta H^\circ_{298} = -351 \ kJ/mol, \quad (17)$$

$$SF_3 + O_2 \rightarrow SO_2F_2 + F, \ \Delta H^\circ_{298} = -260 \ kJ/mol, \quad (18)$$

$$SF_2 + O_2 \rightarrow SO_2F_2, \ \Delta H^\circ_{298} = -461 \ kJ/mol. \quad (19)$$
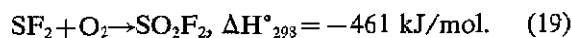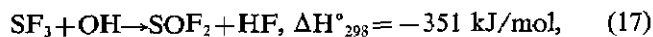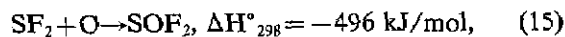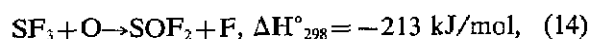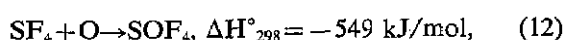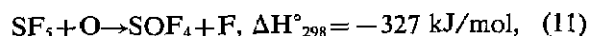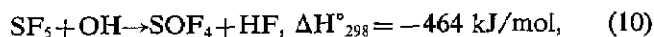
Reactions (13), (14), and (18) have previously been invoked [1,6] to account for rapid SOF_2 and SO_2F_2 formation from pyrolysis of SF_6 in the presence of O_2. Reactions (11)–(14) have been mentioned by d'Agostino and Flamm [8] as mechanisms for oxyfluoride production from SF_6/O_2 mixtures in low-pressure, radio frequency discharges. Reaction (16) has been suggested by Leipunskii et al. [3]. From low-pressure SF_6/O_2 mixtures with relatively high O_2 content there is evidence [21,58,63] that ion and neutral species such as SOF_3^+, $SO_2F_3^+$, $SO_2F_5^+$, $S_3OF_7^+$, SF_5O_2, SF_5O, $SF_5O_2SF_5$, and $SF_5O_3SF_5$ are also formed which may act as intermediates in the production of the observed oxyfluorides. The large, relatively unstable species such as S_2F_{10} and $SF_5O_3SF_5$ could not be observed by the present chromatographic method. It has been argued [58] that for conditions like those considered here, their formation is improbable.

Within the bulk of the gas or on the walls, slower reactions may occur which could modify the gas composition. Processes previously mentioned in this category are:

$$SF_4 + H_2O \rightarrow SOF_2 + 2HF, \ \Delta H^\circ_{298} = -84 \ kJ/mol, \quad (20)$$

$$SOF_4 + H_2O \rightarrow SO_2F_2 + 2HF, \ \Delta H^\circ_{298} = -2 \ kJ/mol, \quad (21)$$

$$SOF_2 + H_2O \rightarrow SO_2 + 2HF, \ \Delta H^\circ_{298} = +54 \ kJ/mol. \quad (22)$$
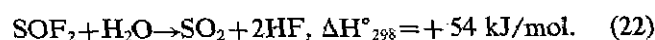
The low rate of SO_2 production and failure to observe significant changes in oxyfluoride content after the gas was undisturbed for long periods suggest that reactions (21) and (22) occur only very slowly if at all in the gas phase at room temperature. Only reaction (20) is rapid enough to influence significantly the observed oxyfluoride production. Its rate has been estimated from measurements of Sauers et al. [20] to lie between 1.0 and 2.6×10^{-19} cm^3/s at a temperature of 350 K. Assuming that this is a gas-phase reaction, and using typical water vapor concentrations found in the present experiments, it is estimated that SF_4 has a half-life in the cell of between 0.15 and 0.40 h. Since this is small compared to typical gas sampling intervals, it can be assumed that SF_4 is completely converted to SOF_2. Reaction (20) has frequently been invoked to account for SOF_2 prod-

uction in previous investigations of SF_6 decomposition; however, it has never been verified that it is actually a gas-phase reaction. If it does occur in the gas phase, then as Herron [65] has suggested it most likely proceeds through the intermediate SF_5OH in two steps.

Because the oxyfluoride concentrations were never permitted to exceed trace levels, it can be presumed that secondary reactions in the small chemically active region were unimportant. These are reactions in which the oxyfluorides are destroyed or undergo conversion from attack by free radicals and ions. It should be noted, however, that secondary ion-molecule reactions involving the expected predominant charge carrier SF_6^- might be significant since these can occur in the larger ion-drift region. One such reaction is the energetically favorable F^- exchange reaction

$$SF_6^- + SOF_4 \rightarrow SOF_5^- + SF_5, \qquad (23)$$
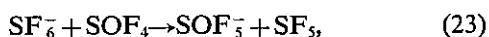
which could affect SOF_4 production. The observed uniformity of production with time suggests, nevertheless, that all secondary reactions are relatively unimportant.

5.3 Interpretation of Results

1. **Influence of O_2 and H_2O.** The sources from which oxygen is derived for formation of SOF_2, SO_2F_2, and SOF_4 have not been positively identified in these experiments, although, as alluded to in the previous section, some processes appear to be more likely than others. The following three sources deserve consideration: 1) gaseous O_2 contamination including that initially present plus that introduced during discharge operation; 2) oxygen contained on surfaces including that which is chemically bound in insulating materials such as SiO_2; and 3) H_2O present either in the gas or on surfaces. Interpretation of the present results in terms of the possible reactions discussed in the previous section suggests that the primary oxygen sources are not necessarily the same for all three species. Because of the high gas pressure and highly confined nature of the discharge which was located far from insulating surfaces, source (2) will be considered unimportant in the discussion that follows.

The data show that oxyfluoride production is not extremely sensitive to variations in the O_2 and H_2O concentratons at levels below 1%. In fact, when the O_2 is higher than 1%, the total oxyfluoride yield actually drops. This suggests that the oxyfluoride yields are controlled mainly by the electron-impact induced dissociation rate of SF_6, i.e., by the availability of SF_x fragments.

The significant drop in SOF_2 yield when O_2 is added can be attributed to at least two possible effects: 1) the

dissociation rate for SF_6 drops when O_2 is added, e.g., due to the influence of O_2 in reducing the mean electron energy within the discharge: and 2) an increasingly greater fraction of SF_4 is consumed by reactions leading to SOF_4 production rather than to SOF_2 production. The first of these is suggested by recent theoretical calculations of electron energy distributions in SF_6/O_2 mixtures by Masek et al. [58]. These calculations, however, pertain mainly to gas mixtures containing larger relative O_2 content than considered here, and there is reason to doubt that the predicted drop in the SF_6 dissociation rate is sufficient to entirely account for the effect reported here. Certainly the second effect can be expected since reaction (12) is energetically favored over reaction (13). However, failure of SOF_4 production to increase significantly when O_2 is added argues against dominance of this effect.

It is in fact conceivable that reactions (13)–(17) are relatively unimportant for SOF_2 formation compared to reaction (20). This is consistent with the observed discharge current dependence for SOF_2 production discussed below which suggests that its formation involves only one molecular dissociation fragment from the discharge. Thus the rate of SOF_2 production could be determined by the rate of SF_4 escape from the active region into the bulk of the gas where reaction (20) occurs. The observed consumption of water vapor might be accounted for by this reaction.

The insensitivity of SO_2F_2 production to variations in low-level O_2 content is more difficult to understand if the predominant mechanisms for its formation involve reactions (18) and (19). Processes such as those involving molecular oxygen are required to account for SO_2F_2 production by a single step mechanism, which, as discussed in the next section, is most consistent with the observed dependence on discharge current. Although other mechanisms for SO_2F_2 formation may be possible, the fact that its production does not drop as precipitously as that for SOF_2 with increasing O_2 content suggests that gas-phase molecular oxygen plays a more important role in its formation. The possible importance of O_2 in enhancing SO_2F_2 yield is suggested by earlier work [3,4,8,15] in which it is reported that in low-pressure discharges addition of O_2 increases SO_2F_2 production at the expense of SOF_4, and in high-pressure arcs O_2 has a much greater influence on SO_2F_2 yield than on SOF_2 yield.

The behavior of SOF_4 production cannot be unambiguously related to either the O_2 or H_2O content because its production is hypothesized here to involve oxygen containing free radicals independent of their source. Failure of SOF_4 to show significant dependence on either O_2 or H_2O content again suggests that the production of active SF_x fragments is the rate deter-

248

mining factor. Certainly some enhancement in the SOF_4 rate can be anticipated by addition of O_2, and this is evidently consistent with the data in figure 17 if allowance is made for a possible reduction in the SF_6 dissociation rate. The overwhelming prevalence of SOF_4 in some diffuse, low-pressure discharges [8] can be understood in terms of the high free radical-to-neutral gas density ratios throughout the gas which would favor its formation according to the mechanisms suggested here.

It is proposed from the foregoing that the dominant oxygen sources for SOF_2 and SO_2F_2 production are derived respectively from H_2O and O_2, whereas SOF_4 can receive oxygen from both of these. Verification of this assignment, however, must await further experiments.

2. Dependence on discharge current.

The condition $dc/dt \propto i$, observed here for SOF_2 and SO_2F_2, is expected if: 1) the formation process involves only one electron-impact-generated dissociation fragment; and 2) changes in i do not significantly modify the electron energy distribution in the discharge. The first condition is satisfied by the mechanisms suggested above that could predominate in SOF_2 and SO_2F_2 production. The second condition is open to question, but is evidently a reasonable assumption [41,47,65,66] for glow or corona-type discharges in which the electric field in the active region is strongly influenced by ion space charge. Increases in applied voltage required to increase the current will presumably expand the volume of space charge without significantly altering the mean E/N. Independent of i and corresponding space-charge development, dissociation is expected to occur predominantly in regions of comparable E/N.

Certainly if $dc/dt \propto i$ for SOF_2 and SO_2F_2, then it is expected, on the basis of the proposed mechanisms, that $dc/dt \propto i^2$ for SOF_4, since its formation involves two fragments from electron-impact dissociation. The production of SOF_4 increases with i as seen in figure 14, but probably somewhat more slowly than i^2. The deviation from i^2 dependence, if significant, could be due to secondary reactions such as reactions (21) or (23) which could remove SOF_4. As production of SOF_4 becomes more predominant, it could affect the production of the other oxyfluorides that compete in the consumption of reactive dissociation products like SF_4 and SF_5. Rates for both SOF_2 and SO_2F_2 show a slow falloff with increasing i which may indicate competition with SOF_4 production. The extent to which SOF_4 production is competitive depends, however, on the extent to which it preferentially consumes free radicals used in SOF_2 or SO_2F_2 formation as opposed to those that would otherwise recombine.

3. Dependence on time.

It has already been noted that a failure of the production curves to exhibit deviations from linearity would tend to indicate that secondary reactions in the active discharge region are relatively unimportant. The present results are consistent with production rates that are constant in time, provided that the initial portions of the production curves can be ignored. Certainly there is no evidence based on the present data to indicate that secondary reactions in the discharge play a dominant role in oxyfluoride production. This is expected because: 1) the concentrations of the gaseous by-products were always at trace levels; and 2) the chemically active volume was much smaller than the main gas volume. The results from gas analysis performed at times after the discharge was extinguished further indicate that secondary reactions in the bulk of the gas are also unimportant. It should be noted, however, that the diminution of secondary reactions may be peculiar to corona discharges, and would certainly not be expected in arcs or diffuse, low-pressure discharges in which a greater fraction of the gas is dissociated.

4. Polarity effect.

The large effect of reversing polarity on the production rates of the oxyfluorides can be understood from consideration of corresponding pronounced changes in the discharge characteristics [40]. In evaluating this effect the following observations are noted: 1) the effect is greater for SO_2F_2 and SOF_4 than for SOF_2; 2) the power dissipation at a given current was always higher for positive polarity; 3) the discharge was more pulsating under positive polarity (see fig. 2); and 4) the point electrode surface suffered considerably more damage under positive polarity. In positive discharges the point electrode surface is evidently subjected to bombardment by more highly energetic ions or electrons from electron avalanches originating in the gas than is the case in negative discharges where a more uniform ion space charge is effective in shielding the electrode surface and moderating the energies of impacting ions. Higher mean electron energies and higher electrode surface temperatures would be consistent with a higher dissociation rate in the positive case. In addition to dissociation by electron impact, pyrolysis of SF_6 at the positive point surface could conceivably contribute to decomposition. The enhancement in oxyfluoride production in going from negative to positive polarity is consistent with the postulated increase in the gas dissociation rate.

Greater heating of the electrode in the positive case could also be accompanied by a higher rate of oxygen release into the discharge volume. This would influence oxyfluoride production and might at least partially account for the more pronounced effect for SO_2F_2 and

249

SOF$_4$, which are likely to be most affected by the presence of oxygen.

5. Magnitude of production rates.

Information is not available at the present time on the rates for all of the various chemical processes which could account for oxyfluoride production. Thus accurate predictions of the production rates are not yet feasible. Nevertheless, sufficient information exists to at least allow upper limits to be placed on the magnitude of the total SF$_6$ decomposition rates for discharges such as considered here in which dissociation is controlled mainly by electron-collision processes.

Based on the evidence offered here that the rate determining factor is the initial SF$_6$ dissociation rate, then an upper limit on the total oxyfluoride production rate can be estimated using the following two assumptions: 1) all SF$_x$ fragments convert to oxyfluorides; and 2) electronic excitation leads predominantly to dissociation so that the total electronic excitation rate k_{ex} coincides with the total dissociation rate. Contributions from ions might also be important, but could be included in the second assumption by making appropriate adjustments in k_{ex}.

For simplicity, a one dimensional approximation is made that electrons are released into the active ionization volume at a constant rate dn_e/dt, e.g., by field emission from the point cathode, and traverse the gap distance d along the point-to-plane axis. These assumptions enable one to compute the total oxyfluoride charge rate of production $r_{q,t}$ defined by

$$r_{q,t} = \sum_{j=1}^{3} r_{q,j}, \qquad (24)$$

where the $r_{q,j}$ are the rates for the individual oxyfluoride components. Allowing for the variations of electron production in the gap by ionization and attachment, one obtains the expression

$$r_{q,t} = i^{-1}(N/N_A)(dn_e/dt) \int_0^d \frac{k_{ex}(l)}{\bar{v}(l)}$$

$$\exp[\int_0^l (\alpha(l') - \eta(l'))dl']dl, \qquad (25)$$

where α and η are respectively the usual ionization and attachment coefficients [41,47], $\bar{v}$ is the electron drift velocity, and N_A is the Avogadro constant required to express the rate in units of moles-per-coulomb. In general, the quantities k_{ex}, $\bar{v}$, α, and η will depend on E/N and hence on position l' in the gap.

Precise variations of E/N within the gap are not easily predicted when the discharge is present due to the expected strong influence of ion space charge on the field. However, the active region near the point in

which significant ionization and excitation occur must satisfy the condition

$$\alpha(l') > \eta(l'). \qquad (26)$$

When this condition no longer holds, electrons are quickly thermalized and removed from the gas by attachment to SF$_6$ molecules. Lacking knowledge of the exact dependence of E/N on l', the active discharge volume will be modeled here as a region of extent l in which eq (26) holds, and E/N assumes a constant value close to the critical value $(E/N)_c$ where $\alpha = \eta$. This choice takes into consideration the expected moderating effect of the ion space charge which tends to reduce the field near the point.

Expressing N in terms of pressure P and temperature T using $N = P/kT$ (k is the Boltzmann constant), the approximation for $r_{q,t}$ becomes

$$r_{q,t} \simeq \frac{k_{ex}Pl}{e\bar{v}kT}\left(\frac{1}{N_0}\right), \qquad (27)$$

where e is the electron charge, and k_{ex} and $\bar{v}$ assume the values for the mean electronic-excitation-rate coefficient and drift velocity respectively at $E/N = (E/N)_c = 370 \times 10^{-21}$ Vm^2 corresponding to the known [67] critical value for SF$_6$. In deriving eq (27) it is assumed that the measured discharge current i corresponds to electron motion only. The parameter l is possibly pressure dependent since it is known [41,47] that the extent of the active discharge region contracts with increasing gas pressure for corona discharges. Thus the pressure dependence implied in eq (27) does not hold in general.

There appears to be some disagreement in the literature [48,49,68] about the correct total electronic-excitation cross sections needed to determine the rate coefficient k_{ex} for SF$_6$. It will be assumed here that 2×10^{-15} m^3/s $\geqslant k_{ex} \geqslant 1 \times 10^{-15}$ m^3/s, where the lower value corresponds to that calculated by Masek et al. [57] at $E/N = 100 \times 10^{-21}$ Vm^2 and the upper value allows for the expected increase in k_{ex} for $E/N = (E/N)_c$. The values of k_{ex} considered here are comparable in magnitude to those reported in the literature for other molecules [69]. The observed [67,70] value for $\bar{v}$ in SF$_6$ at $(E/N)_c$ is about 2×10^5 m/s. The extent of the active region is expected [40] to lie between about 1 and 2% of the total gap spacing, i.e., for the present case, 0.24 mm $> l > 0.12$ mm. Using eq (27), the predicted upper limit on the rate for a pressure of 200 kPa and temperature of 300 K lies in the range, 1800 μmoles/C $> r_{q,t} > 450$ μmoles/C. This can be compared with the value obtained from tables 3–5 for a pressure of 200 kPa. For positive discharges at 8.0 μA and 16.0 μA

250

respectively it is found, for example, that $r_{q,t}=634$ μmoles/C and $r_{q,t}=717$ μmoles/C, and for a negative discharge at 40 μA, $r_{q,t}=96$ μmoles/C.

The results for positive discharges generally lie within the range of predicted upper limit values whereas results for negative discharges lie well below the range. The model used is perhaps more relevant to negative discharges where electrons originate from the point electrode surface and the space charge is expected to be uniformly distributed about the point. The space charge for positive discharges is probably less uniform, and as previously suggested, there may be contributions to dissociation from processes other than electron impact. Undoubtedly, the appropriate mean value of E/N in the active volume is greater than $(E/N)_c$ for the positive case. However, independent of polarity, the total rates $r_{q,t}$ should not lie significantly above the range of upper limits estimated here.

6. Conclusions

The oxyfluorides SOF_2, SO_2F_2, and SOF_4 have been identified as the major stable gaseous by-products from highly localized, low-current corona discharges in SF_6 containing trace levels of O_2 and H_2O for total gas pressures from 100 kPa to 300 kPa. The absolute charge and energy rates-of-production for these species were measured for different discharge conditions and found to be below the theoretically estimated upper limits and comparable in magnitude to rates previously determined for other types of electric discharges in SF_6. From considerations of the dependences of the rates on varying O_2 and H_2O content, it has been possible to conclude that the controlling rate factor is the SF_6 dissociation rate in the discharge.

The charge rates-of-production for both SOF_2 and SO_2F_2 are found to be nearly independent of current, suggesting formation mechanisms for these species that involve only one fragment from molecular dissociation in the discharge. Interpretation of this observation in terms of possible reactions further suggests that SOF_2 and SO_2F_2 respectively derive their oxygen predominantly from gas-phase H_2O and O_2. The charge rate-of-production for SOF_4 is observed to increase with current, thus suggesting a predominant mechanism for its formation involving more than one molecular dissociation fragment.

Gas analysis performed before and after the decomposed gas was left undisturbed for many hours showed that hydrolysis of SOF_4 leading to SO_2F_2 formation is too slow to observe in the gas phase and therefore cannot account for SO_2F_2 production as suggested by some earlier investigators. Hydrolysis of SOF_4 could nevertheless occur rapidly on surfaces, and this process may

account for a failure to observe this species in some previously reported experiments on corona discharges in SF_6. The present results indicate that hydrolysis of SOF_2 in the gas phase is also not important. The observed uniformity of the production rates with time argues against significant influence from any secondary reactions involving the oxyfluorides.

The absolute production rates reported here are presently the most accurate available, and should prove useful in estimating detection sensitivities needed to design chemical diagnostics for practical SF_6-insulated high-voltage systems. It should be cautioned, however, that there may be difficulties in applying the present results to ac corona because of the rather large polarity effect which has been observed. The data offered can at least permit upper and lower bounds to be placed on oxyfluoride production in ac discharges.

References

[1] Siegel, B., and P. Breisacher, J. Inorg. Nucl. Chem. 31, 675 (1969).

[2] Padma, D. K., and A. R. Vasudeva Murthy, J. Fluor. Chem. 5, 181 (1975).

[3] Leipunskii, I. O.; A. K. Lyubimova, A. A. Nadeikin, A. I. Nikitin and V. L. Talroze, Sov. J. Quantum Electron. 12, 413 (182).

[4] Velichko, A. M.; I. O. Leipunskii, A. K. Lyubimova, A. A. Nadeikin, A. I. Nikitin, and V. L. Talroze, High Energy Chem. 17, 124 (183).

[5] Ambartsumyan, R. V.; Yu. A. Gorokhov, V. S. Letokhov, G. N. Makarov, and A. A. Puretskii, Sov. Phys. JETP 44, 231 (1976); Sov. Phys. JETP 42, 993 (1976).

[6] Wray, K. L., and E. V. Feldman, J. Chem. Phys. 54, 3445 (1971); Proc. 14th Int. Symp. on Combust. 229 (1972).

[7] Gilbert, R.; J. Castonguay and A. Theoret, J. Appl. Poly. Sci. 24, 125 (1979).

[8] d'Agostino, R., and D. L. Flamm, J. Appl. Phys. 52, 162 (1981).

[9] Bruno, G.; P. Capezzuto and F. Cramarossa, J. Fluor. Chem. 14, 115 (1979).

[10] Emeleus, H. J., and B. Tittle, J. Chem. Soc. 1644 (1963).

[11] Hirooka, K.; H. Kuwahara, M. Noshiro, and Y. Jitsugiri, Elec. Eng. Japan 95, 14 (1975).

[12] Manion, J. P.; J. A. Philosophos and M. B. Robinson, IEEE Trans. Elec. Insul. **2**, 1 (1967).

[13] Ruegsugger, W., and F. K. Kneubuhl, Appl. Phys. **B31**, 9 (1983).

[14] Grasselt, H.; W. Ecknig, and H. J. Polster, Elektrie **32**, 369 (1978).

[15] Boudene, C.; J. Cluet, G. Keib, and G. Wind, Rev. Gen. Electr. No. Special, 45 (1974); B. Bouvier and G. Wind, Rev. Gen. Electr. **86**, 773 (1977).

[16] Baker, A.; R. Dethlefsen, J. Dodds, N. Oswalt, and P. Vouros, Elec. Power Res. Inst. Rept., EPRI-EL1648 (1980).

[17] Chu, F. Y., and R. E. Massey, *Gaseous Dielectrics III*, Proc. 3rd Int. Symp. on Gaseous Dielectrics (Pergamon, New York 1982) pp. 410–417.

[18] Chu, F. Y.; H. A. Stuckless and J. M. Braun, *Gaseous Dielectrics IV*, Proc. 4th Int. Symp. on Gaseous Dielectrics (Pergamon, New York, 1984) pp. 462–472.

[19] Becher, W., and J. Massonne, Elektrotech. Z. Ausg. **A91**, 605 (1970).

[20] Sauers, I.; H. W. Ellis, L. C. Frees, and L. G. Christophorou, *Gaseous Dielectrics III*, Proc. 3rd Int. Symp. on Gaseous Dielectrics (Pergamon, New York, 1982) pp. 387–401; IEEE Trans. Elec. Insul. **EI-17**, 284 (1982).

[21] Frees, L. C.; I. Sauers, I. W. Ellis, and L. G. Christophorou, J. Phys. D: Appl. Phys. **14**, 1629 (1981).

[22] Castonguay, J., Conf. Record, IEEE Int. Symp. on Elect. Insul., Boston (1980).

[23] Gutbier, H., Phys. Verh. **17**, 163 (1966).

[24] Waddington, F. B., and J. Heighes, AEI Eng. **7**, 196 (1967).

[25] Bartakova, B.; J. Krump and V. Vosahlik, Electrotechnicky Obzor. **67**, 230 (1978).

[26] Ophel, T. R.; D. C. Weisser, A. Cooper, L. K. Fifield, and G. D. Putt, Nuc. Instrum. and Methods **217**, 383 (1983).

[27] Thorburn, R., Nature **175**, 423 (1955).

[28] Edelson, D.; C. A. Bieling and G. T. Kohman, Indust. Eng. Chem. **45**, 2094 (1953).

[29] Schumb, W. C.; J. G. Trumb and G. L. Priest, Indust. Eng. Chem. **41**, 1348 (1949).

[30] Frost, D. C.; S. T. Lee, C. A. McDowell, and N. P. C. Westwood, J. Elec. Spec. and Rel. Phenomena **12**, 95 (1977).

[31] Kusumoto, S. Itoh, Y. Tsuchiya, H. Mukae, S. Matsuda, and K. Takahushi, IEEE Trans. Power Appar. Syst. **PAS-99**, 1456 (1980).

[32] Tahiliani, V. H.; K. B. Miners and W. J. Lannes, Proc. Int. Conf. on Large High Voltage Electric Systems (CIGRE, 1984).

[33] Latour-Slowikowska, H.; J. Lampe and J. Slowikowski, *Gaseous Dielectrics IV*, Proc. 4th Int. Symp. on Gaseous Dielectrics (Pergamon, New York, 1984) pp. 286–291.

[34] Tominaga, S.; H. Kuwahara and K. Hirooka, IEEE Trans. Power Appar. Syst. PAS-98, 2107 (1979).

[35] Suzuki, T.; S. Nakayama and T. Yoshimitsu, IEEE Trans. Elec. Insul. **EI-15**, 53 (1980).

[36] Vijh, A. K., IEEE Trans. Elec. Insul. **EI-11**, 157 (1976).

[37] Van Brunt, R. J., and D. A. Leep, *Gaseous Dielectrics III*, Proc. 3rd Int. Symp. on Gaseous Dielectrics (Pergamon, New York, 1982) pp. 402–409.

[38] Van Brunt, R. J.; T. C. Lazo and W. E. Anderson, *Gaseous Dielectrics IV*, Proc. 4th Int. Symp. Gaseous Dielectrics (Pergamon, New York, 1984) pp. 276–285.

[39] Sauers, I.; L. G. Christophorou and S. M. Spyrou, *Gaseous Dielectrics IV*, Proc. 4th Int. Symp. Gaseous Dielectrics (Pergamon, New York, 1984) pp. 292–305; L. G. Christophorou, I. Sauers, D. R. James, H. Rodrigo, M. O. Pace, J. G. Carter, and S. R. Hunter, IEEE Trans. Elec. Insul.

EI-19, 550 (1984).

[40] Van Brunt, R. J., and D. Leep, J. Appl. Phys. **52**, 6588 (1981); R. J. Van Brunt and M. Misakian, IEEE Trans. Elec. Insul. EI-17, 106 (1982); J. Appl. Phys. **54**, 3074 (1983).

[41] Sigmond, R. S., in *Electrical Breakdown of Gases*, edited by J. M. Meek and J. D. Craggs (Wiley, New York, 1978), pp. 319–384.

[42] Van Brunt, R. J., *Proc. 7th Int. Conf. Gas Discharges and Their Applications* (Peter Peregrinus, 1982), pp. 255–258.

[43] Dudley, F. B.; G. H. Cady and D. F. Eggers, J. Am. Chem. Soc. **78**, 1553 (1956).

[44] DesMarteau, D. D., Clemson University, private communication.

[45] Hasegawa, S.; L. Greenspan, J. W. Little, and A. Wexler, *A Laboratory Study of Some Performance Characteristics of An Aluminum Oxide Humidity Sensor*, NBS Tech. Note 824, 1974; F. Ansbachera nd A. C. Jason, Nature **171**, 177, (1953); A. C. Jason and J. L. Wood, Proc. Phys. Soc. (London) **B68**, 1105 (1955).

[46] Van Brunt, R. J., and M. C. Siddagangappa, Proceedings of the 37th Gaseous Electronics Conference, Bull. Am. Phys. Soc. **30**, 132 (1985).

[47] Goldman, M., and A. Goldman, in *Gaseous Electronics*, edited by N. M. Hirsh and H. J. Oskam (Academic, New York, 1980), vol. 1, p. 219–290; A. Goldman and J. Amourouz, in *Electric Breakdown and Discharges in Gases*, edited by E. E. Kunhardt and L. H. Luessen (Plenum, New York, 1981), pp. 293–346.

[48] Yoshizawa, T.; Y. Sakai, H. Tagashira, and S. Sakamoto, J. Phys. D: Appl. Phys. **12**, 1839 (1979); H. Itoh, M. Shimozuma, and H. Tagashira, J. Phys. D: Appl. Phys. **13**, 1201 (1980).

[49] Kline, L. E.; D. K. Davies, C. L. Chen, and P. J. Chantry, J. Appl. Phys. **50**, 6789 (1979).

[50] Dincer, M. S., and G. R. Govinda Raju, J. Appl. Phys. **54**, 6311 (1983).

[51] Modica, A. P., J. Phys. Chem. **77**, 2713 (1973).

[52] Hay, P. J., J. Am. Chem. Soc. **99**, 1003 (1977).

[53] Hildenbrand, D. L., J. Phys. Chem. **77**, 897 (1973).

[54] Babcock, L. M., and G. E. Streit, J. Chem. Phys. **74**, 5700 (1981).

[55] Kiang, T., and R. N. Zare, J. Am. Chem. Soc. **102**, 4024 (1980).

[56] Dibeler, V. H., and J. A. Walker, J. Chem. Phys. **44**, 4405 (1966).

[57] Masek, K.; L. Laska, V. Perina, and J. Krasa, Acta. Phys. Slov. **33**, 145 (1983).

[58] Gonzalez, A. C., and H. J. Schumacher, Z. Naturforsch. B: Anorg. Chem., Org. Chem. **36B**, 1381 (1981).

[59] Wilkins, R. L., J. Chem. Phys. **51**, 853 (1969).

[60] K. P. Brand, K. P., and J. Kopainsky, Appl. Phys. **16**, 425 (1978).

[61] Bott, J. P., and T. A. Jacobs, J. Chem. Phys. **50**, 3850 (1969).

[62] The enthalpies of reactions listed apply only at 298 K and in some cases are only approximate due to possible large uncertainties in the heats of formation of species like SF_2, SF_3, SOF_2, and SOF_4 (J. T. Herron, National Bureau of Standards, private communication). The values given were derived from several sources including references [1, 3,] and JANAF Thermochemical Tables, J. Phys. Chem. Ref. Data **7**, 917 (1978); **3**, 387 (1974); D. D. Wagman, W. H. Evans, V. B. Parker, R. H. Schumm, I. Halow, S. M. Bailey, K. L. Churney, and R. L. Nuttall, J. Phys. Chem. Ref. Data **11**, Suppl. on 2 (1982).

[63] Gonzalez, A. C., and H. J. Schumacher, Zeit. Phys. Chem. **127**, 167 (1981); J. Czarnowski and H. J. Schumacher, Int. J.Chem. Kinetics **11**, 613 (1979).

252

[64] Herron, J. T., *Gaseous Dielectrics IV*, Proc. 4th Int. Symp. Gaseous Dielectrics (Pergamon, New York, 1984) pp. 273–274.
[65] Kelley, E. F., and R. E. Hebner, J. Appl. Phys. **52**, 191 (1981).
[66] Aleksandrov, G. N., Sov. Phys. Tech. Phys. **8**, 161 (1963).
[67] Gallagher, J.; E. C. Beaty, J. Dutton, and L. C. Pitchford, J.

Phys. Chem. Ref. Data **12**, 109 (1983).
[68] Novak, J. P., and M. F. Frechette, J. Appl. Phys. **55**, 107 (1984).
[69] Dutton, J., J. Phys. Chem. Ref. Data **4**, 577 (1975).
[70] Naidu, M. S., and A. N. Prasad, J. Phys. D: Appl. Phys. **5**, 1090 (1972).

APPENDIX

Examples of values for the parameters in eq (8) for $c(Q)$ which were obtained from fits to data for SOF_2 and SO_2F_2 are given in table 7. Also indicated in this table are the maximum values for net charge transported, Q_{max}, to which these fits apply. Instantaneous production rates $r_q'(Q)$ at particular values of Q can be calculated using

$$r_q'(Q) = (1+\epsilon)AQ^\epsilon, \qquad (A1)$$

which is derived from eq (8). Values for some rates computed in this way have previously been reported [38].

Fits to concentrations plotted versus energy dissipated yielded curves of essentially the same shape, i.e., $\epsilon' \simeq \epsilon$ and $c_0' \simeq c_0$. The values of A and A' depend, of course, on the different units in which the rates are expressed. The limiting, uniform rates r_q in tables 3 and 4 are generally slightly less than those calculated from eq (A1) at $Q = Q_{max}$. The rates r_q are obtained from linear, least-squares fits ($\epsilon = 0$ in eq (8)) to the data for $Q_{max} \geqslant Q \geqslant Q_{min}$, where Q_{min} is the lowest value of net accumulated charge at which the assumption of linearity holds. If $\epsilon \simeq 0$, as in the case of some SOF_4 data, then $r_q \simeq A$. It was found for all cases reported that $2r_q > 2A > r_q$.

Table 7. Values of parameters obtained from fits of the form given by eq (8) for $c(Q)$.

Species	Polarity	Pressure (kPa)	Current (μA)	c_0	A	ϵ	$Q_{max}(C)$
SOF_2	Pos.	116	20.0	2.08×10^{-7}	2.32×10^{-5}	0.579	1.90
		200	1.5	9.28×10^{-7}	2.05×10^{-4}	0.449	0.40
		200	8.0	2.96×10^{-6}	2.45×10^{-4}	0.541	0.40
		200	16.0	3.04×10^{-11}	2.07×10^{-4}	0.634	0.48
		300	8.0	2.29×10^{-11}	1.92×10^{-4}	0.696	0.54
		300	16.0	1.06×10^{-6}	1.21×10^{-4}	0.684	0.93
	Neg.	114	25.0	6.77×10^{-7}	3.04×10^{-5}	0.250	2.42
		200	16.0	1.67×10^{-6}	2.46×10^{-5}	0.208	2.30
		200	40.0	2.37×10^{-7}	2.03×10^{-5}	0.227	2.74
		300	16.0	1.37×10^{-6}	1.96×10^{-5}	0.386	2.35
		300	21.0	8.32×10^{-7}	1.54×10^{-5}	0.166	3.01
SO_2F_2	Pos.	116	20.0	4.59×10^{-8}	3.14×10^{-5}	0.633	1.90
		200	1.5	1.41×10^{-6}	2.06×10^{-4}	0.583	0.40
		200	8.0	2.61×10^{-6}	1.70×10^{-4}	0.490	0.40
		200	16.0	2.67×10^{-12}	1.16×10^{-4}	0.477	0.48
		300	8.0	6.46×10^{-11}	1.16×10^{-4}	0.393	0.54
		300	16.0	$\sim 1 \times 10^{-14}$	0.75×10^{-4}	0.529	0.93
	Neg.	114	25.0	2.47×10^{-6}	0.92×10^{-5}	0.486	2.42
		200	16.0	1.59×10^{-11}	1.20×10^{-5}	0.243	2.30
		200	40.0	2.03×10^{-6}	1.03×10^{-5}	0.204	2.74
		300	16.0	2.27×10^{-6}	0.92×10^{-5}	0.474	2.35
		300	21.0	3.72×10^{-12}	0.63×10^{-5}	0.586	3.01

A High Temperature, High Pressure Reaction-Screening Apparatus

Thomas J. Bruno and Gretchen L. Hume

National Bureau of Standards, Boulder, CO 80303

This short note describes an apparatus that has been designed and constructed to allow assessment of the extent of chemical decomposition of fluids and fluid mixtures under high temperature, high pressure conditions. The apparatus is used to screen fluid systems prior to PVT (pressure-volume-temperature) or VLE (vapor-liquid equilibrium) experiments under severe conditions. For a predetermined residence time, the fluids are maintained at the temperature and pressure at which the PVT or VLE experiment will be conducted. The residence time in the reactor is comparable to the expected residence time in the PVT or VLE apparatus. Samples of fluid are withdrawn directly at regular intervals for analysis by gas chromatography, or collected in a sampling vessel for more extensive analysis.

Key words: decomposition; high pressure; high temperature; reactions.

1. Introduction

Recently there has been an increasing amount of interest in obtaining pressure-volume-temperature (PVT) data and vapor-liquid equilibrium (VLE) data for fluids and fluid mixtures at high temperature and high pressure. This is due to the importance of these properties in engineering design and process development [1–5][1]. An inadequate knowledge of these parameters is costly to industry in financial terms [6–12]. Specifically, PVT and VLE measurements are necessary for fluids and fluid mixtures at temperatures greater than 200 °C and pressures greater than 30 MPa, but under these conditions the possibility of decomposition or reaction of the fluids and fluid mixtures is very real. We must therefore con-

sider the thermodynamic, kinetic, and catalytic factors which are involved. Thermodynamic factors include activation energies and equilibrium positions [13]. The primary kinetic consideration is the strong temperature dependence of the rate constant [14]. The construction materials, wetted by the fluids in the experimental measurement apparatus, are often responsible for catalytic effects. Further, since many fluids become highly corrosive under severe conditions, the possibility of damage to instrumentation must also be taken into account.

It is clearly important to assess the possibility and extent of reactions of test fluids in PVT and VLE experiments [3]. Further, it is important to address this issue before the experiments are actually attempted.

The reaction screening apparatus described in this note is a simple apparatus easily constructed from commercially available materials.

2. Apparatus Description

The reaction screening apparatus is shown schematically in figure 1. The heart of the apparatus is a small, thick-walled pressure vessel which serves as the reaction chamber. This vessel was machined from a sec-

[1]Numbers in brackets indicate literature references.

High Pressure Reaction Apparatus

To Vent

Sample Gas Inlet Valves

Pressure Gauge

Reference Thermocouple

DVM

Inert Gas to Vent

Rupture Disk

Vent Valve

Cut Off Valve

J Type Termo-couple

Check Valve

Vacuum Valve

Loop Inlet Valve

Reaction Vessel

Carrier Gas Inlet

To Vacuum

4 Port Valve

Ext. Sample Cyl.

To Chromatograph

Pressure Gauge

T_c

Rotameter

Reaction Vessel Thermostat (negative pressure)

Inert Purge Gas Inlet
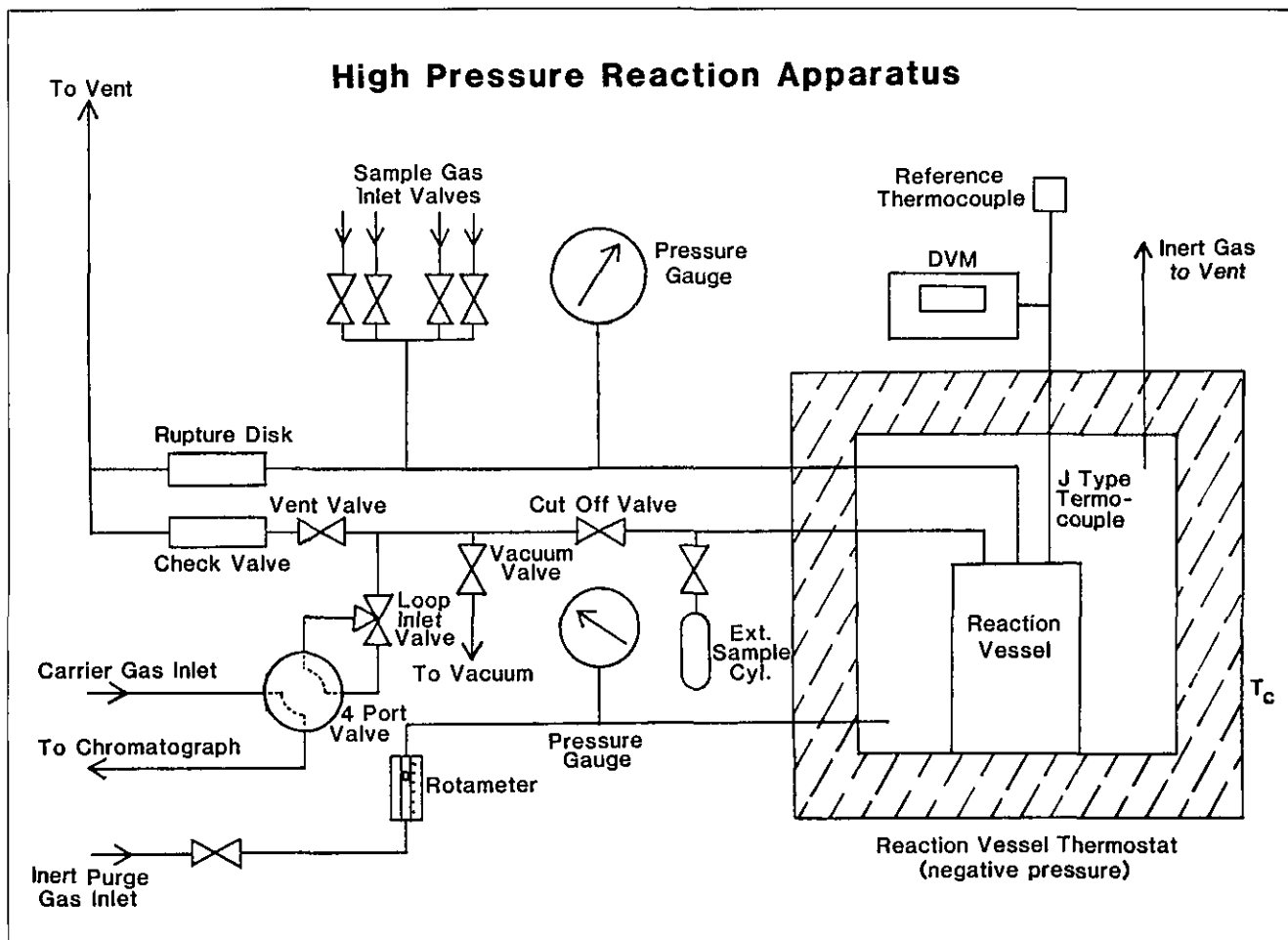
Figure 1–Schematic diagram of the reaction screening apparatus.

tion of work-hardened 316L stainless steel (AISI designation) barstock, and can withstand a pressure of 130 MPa at 250 °C. Tolerances and specifications of this vessel exceed the requirements set forth by the ASME [15]. The cover of the vessel, secured using a bolted closure, contains feedthroughs for introducing the test fluids and removing samples for analysis. Sealing is provided by a gasket of either 316 SS or 25% glass filled PTFE. A thermowell is provided in the vessel to contain a J-type (iron-constantan) thermocouple, the referenced output of which is displayed on a digital voltmeter (DVM in fig. 1).

The pressure vessel rests within an aluminum jacket containing cartridge heaters (not shown in fig. 1). This heating apparatus maintains a constant temperature in the pressure vessel and minimizes temperature gradients.

The pressure vessel, enclosed in the aluminum jacket, is contained in a convection oven (T_c on fig. 1) specifically designed and built for this application. The oven is internally insulated with bonded mineral wool board.

The outer casing of the oven is of welded seam construction with a PTFE gasket providing the door seal. It is maintained at a slight negative pressure by a dedicated blower system, and is equipped with an inert gas purge line. A nondefeatable safety head containing a 68 MPa rupture disk provides over-pressure protection. A combustible gas detector and an electrochemical detector [16] are located nearby to provide additional safety.

Sampling of the contents of the pressure vessel can be done in two ways during the course of a screening test. The sample line is directly connected to a chromatographic four port sampling valve which is in turn connected to an analytical chromatograph. The sampling valve has another three port valve interposed in the sampling loop. This arrangement allows the valve and sample loop to be evacuated before filling, and allows a minimum amount of sample to be expended for each analysis, since the need for purging is minimal.

Alternatively, an external sampling cylinder may be filled with the test fluid and the analysis done off line. This makes possible the use of mass spectrometry and

256

spectrophotometry, as well as more specific tests.

The apparatus has been used successfully (in conjunction with a direct fugacity measurement system) [17] for over a year. In this application, gaseous mixtures containing hydrogen in binary mixtures with industrially important gases (such as methane, propane, carbon dioxide and carbon monoxide) are tested for reaction with a palladium/silver alloy. This alloy is a construction component of the fugacity apparatus, and under certain conditions of temperature and pressure may act as a catalyst. The reaction screening apparatus has been used to determine the conditions under which decomposition or reaction might occur. The apparatus is also used to determine the effect of test fluids on the palladium/silver component, since many compounds (olefins, organic sulfur compounds, higher hydrocarbons) can damage the alloy under severe conditions.

The reaction screening apparatus is a versatile lab scale semibatch or batch reactor. In it, a variety of fluids and fluid mixtures can be tested with or without catalysts at various temperatures and pressures. Using the reactor in conjunction with the gas chromatograph, reactions, decomposition and nominal rate of reaction data may be obtained.

References

[1] Straty, G. C., and A. M. F. Palavra, J. Res. Natl. Bur. Stand. (U.S.) 89(5): 1 (1984).

[2] Machado, J. R. S., and W. B. Streett, J. Chem. Eng. Data 28: 218 (1983 and references therein).

[3] Hanley, H. J. M., Position statement on experimental procedures for chemically reacting fluids. Chemical Engineering Science Division, private communication (Sept. 1984).

[4] Sengers, J. V., and M. Klein, The importance of accurate thermophysical property information, Natl. Bur. Stand. (U.S.) Special Pub. 590; Washington, DC (1980).

[5] Lide, D. R. Science 212: 1343 (1981).

[6] O'Reilly, M. G., and B. Edmunds, The Chem. Eng.; Jan. 1978; p. 61.

[7] Zudkevitch, D. Hyd. Proc. 54: 97 (1975).

[8] Yen, L. C.; J. F. S. Frith, K. C. Chao, H. M. Lin, Chem. Eng. 84: 127 (May 1977).

[9] Williams, C. C. and M. A. Albright, Hyd. Proc. 55: 115 (1976).

[10] Maddox, R. N.; D. Zudkevitch and J. H. Erbar, ASME 82-WA/HT-59.

[11] Zudkevitch, D. Forensic thermodynamics. In phase equilibria and fluid properties in the chemical industry. Proceedings 2nd Int. Conf.; Frankfurt AM, West Germany: Dechema (1980).

[12] Hale, D. Pipeline Gas J. 201(8); 26 (July 1974).

[13] Wall, F. T. Chemical thermodynamics. San Francisco: W. H. Freeman Company (1974).

[14] Nicholas, J. Chemical kinetics. New York: John Wiley & Sons (1976).

[15] ASME Boiler and Pressure Vessel Code, Sec. VIII: Unfired Pressure Vessels. New York: American Society of Mechanical Engineers (1965).

[16] Auel, R. Sensors 1: 9 (1984).

[17] Bruno, T. J. J. Res. Natl. Bur. Stand. (U.S.) 90 (2): 127 (1985).

WAYS TO STANDARDIZATION IN ELECTROPHORESIS ARE BROUGHT TO LIGHT

A workshop entitled Electrophoresis Standardization: Approaches and Needs, drew 54 participants to the National Bureau of Standards (NBS) June 25,1984. Co-sponsored by NBS and the Electrophoresis Society of the Americas, the meeting was hosted by the NBS Center for Analytical Chemistry.

The participants, many of whom came in conjunction with an International Symposium on Electrophoresis in Quantico, VA, organized by the Federal Bureau of Investigation, represented leadership in various scientific sectors. They included 15 representatives from industry and 8 from universities with the remainder from government agencies including State crime laboratories, the National Institutes of Health, the Uniformed Services University of the Health Sciences, and the Food and Drug Administration.

The first series of talks discussed various needs for standardization. Subsequent talks described how different laboratories approach standardization. Summaries of some of the talks are given in this review. A monograph containing edited versions of the papers was scheduled for release this spring.

Dr. Robert Allen, Medical University of South Carolina, gave an introductory talk that addressed some of the current directions in electrophoresis. The recent mandates by many states to perform electrophoresis on the blood of newborns will have a dramatic impact on the need for interlaboratory comparisons. This suggests also that there will be needs for standardized materials, standard protein mixtures, and specifications for materials purity.

Dr. Berthold Radola, visiting from the Technische Universität München, Federal Republic of Germany, discussed an important new concept for the standardization of thin layer isoelectric focusing (TL-IEF). He described a new technique for bonding and drying acrylamide on a polymer film. One variable in TL-IEF techniques is the unpredictable starting condition of voltage and current flow because of varying amounts and types of impurities present in the casting mixtures due to different acrylamide sources.

Preparation of acrylamide gels involves polymerization of acrylamide and results in variable amounts of persulfate in the gel. The process of bonding and drying acrylamide for producing rehydratable gels includes a series of washes that removes unpolymerized material, impurities, and excess persulfate from the casting mixture. The resulting TL-IEF medium is rehydrated in the appropriate ampholyte mixture to produce gels that give reproducible results. The initial voltages are greater and focusing times can be shortened because of higher field strengths. The availability of these materials from a commercial source should allow many laboratories to be able to perform TL-IEF analyses using comparable gel substrates.

Dr. Bruce Budowle from the Federal Bureau of Investigation described a modified procedure for determining phenotypes of phosphoglucomutase. This enzyme is important in the forensic field because of the possibility of discriminating certain individuals from others on the basis of blood stains found at the scene of a crime of violence. The initial procedure developed was reproducible based on results from over 100 runs. However, changes occurred in the banding patterns after the deionizing cartridge in the purified water system was changed. It appears that contaminants in the original system were helping to achieve the original, reproducible separations. With a highly purified water (10–14 megohm resistivity), reproducibility was lost. This is particularly disturbing because the original results could not be reproduced by adding back known impurities such as sodium chloride. However, it was generally suggested that reproducibility depended upon the capability of having a known, controlled system and that defining electrophoretic solutions based upon the purest water was the best approach.

Dr. Carl Merril of the National Institutes of Health described the historical aspects of the development of the silver stain for electrophoretic gels. He also gave evidence for a number of mechanisms by which silver stain works. He suggested that the standardization of a silver stain was going to be difficult because of the variety and combination of stains and electrophoretic separations used in laboratories today and the reluctance of laboratories to switch from a system they are accustomed to using. However, he sug-

gested that one of the more promising ways to achieve standardization is the use of a normalization procedure for doing quantitative work and the development and use of standardized protein methods for absolute quantitation.

One of the difficulties in quantitation is making sure that the stained protein spots are not saturated with silver. A result of saturation is that the tops of the densitometric tracings are "clipped"; consequently, there is no Gaussian distribution of stain in the spot. Linear results can be achieved if precautions are taken to make sure that the proteins are not saturated. Each protein has a different linear calibration curve which means that the relationship of each protein to a standard has to be known. Thus, in comparing spots on two dimensional gels or bands on one-dimensional gels, it is necessary to compare the same respective protein spots or bands on different gels. One way to overcome variations in quantitation between gels is to choose a set of spots on two-dimensional gels that have the same density ratios from one gel to the next. These spots are called operationally consistent. The characteristic values of these spots are then taken to develop a correction factor so that all spots on a gel can be normalized against that set of spots. Individual variations between spots can then be detected and protein changes determined.

The concentration of individual proteins can change for a number of reasons. For example, some human proteins change in a subtle manner as people age. Three known proteins that increase with age are actin, apo-al-lipoprotein, and haptoglobin. Haptoglobin con-

---

. . . the pattern in the gel could be used in much the same way as a photographer uses a step wedge.

---

centration increases approximately 43% per decade of life. Some proteins are observed to change when a person contracts Parkinson's disease while others may be expressed as the result of an individual contracting multiple sclerosis.

Dr. Merril suggested that a useful standard could be obtained by carbamylating proteins to produce electrophoretically separated spots of a fixed pattern in an electrophoretic gel. By increasing the concentration of each protein, the pattern in the gel could be used in much the same way as a photographer uses a step wedge. The difficulty with this process is that one would have to make sure that all proteins remained in the gel. One way to correct for such variations is to label radioactively the proteins to provide a second technique to check for protein penetration into the gels. By making

appropriate corrections, relative concentrations could be replaced with absolute concentration.

Richard Cook the FMC Corporation discussed applications of agarose in gel diffusion, electrophoresis, chromatography, and cell culture and the requirements for an agarose for use in each of those applications. The requirements for an agarose can be defined in terms of measurable parameters, including clarity, electroendoosmosis (correlated with the amount of ester sulfate), gel strength, various polyanions and their associated hydrated cations, pyruvate, moisture, and gelling temperature. Because many laboratories have specialized needs for certain properties of agarose, it is impractical to narrow the choices to a single type of agarose. However, with the ability to furnish analytical data for each lot of material, along with an assurance that lot-to-lot variations will be minimal, the industry could provide the researcher with valuable information with which intelligent choices can be made.

Dr. Norman Anderson, Argonne National Laboratories, discussed aspects of standardization that affect

---

. . . tighter manufacturing standards would help to avoid currently observed differences.

---

two-dimensional electrophoresis. He presented results showing standardization of the first dimension separation by isoelectric focusing through the use of carbamylated creatine phosphokinase. These carbamylated proteins differ from one another by a single charge. Use of these proteins yields information about the ampholytes incorporated in the gels to create the pH gradient. Dr. Anderson showed that different manufacturers' lots of ampholytes produced variable spacing of the separated proteins throughout the isoelectric focusing gel. He selected and procured a large batch of ampholytes that showed the most even spacing in the gel. While this is one way to achieve reproducible run-to-run results, tighter manufacturing standards would help to avoid currently observed differences. In addition, standards (pI markers) are still needed to extend the range of proteins into the basic and acidic ends of the isoelectric focusing gel. Currently available pI markers are still limited in their pH range.

For molecular weight standardization, Dr. Anderson's laboratory uses a homogeneous preparation of rabbit psoas muscle, mainly because many of the rabbit proteins have been sequenced and molecular properties have been described.

Resolution of a two-dimensional gel is more difficult to measure. One approach is to take an average of all the spots on the gel and determine how many

average-sized spots can be packed into the gel and still maintain resolution. This theoretical measurement gives an indication of how different modifications to the system will improve or degrade performance.

Dr. Anderson then discussed problems in matching distorted gels and in the presentation of data. Pattern recognition is an emerging technology for two-dimensional electrophoresis, with the emphasis being placed on identification of individual protein spots.

Dr. George Bers, Bio-Rad Inc., presented information from a thorough literature review of the detergent sodium dodecyl sulfate (SDS) and its effects in electrophoresis. He classified the various potential contaminants of SDS and showed examples of how electrophoresis is affected. He also pointed out the several types of lipophilic contaminants such as the lower alkyl alcohols, alkene hydrocarbons, and the di-alkyl ethers. There are other potential contaminants such as the dialkyl sulfates and alkyl acids that are generally insoluble and tend to show their presence in terms of a cloudy SDS preparation. Other contaminants mentioned were inorganic salts, metals, amino acid contaminants fromfibers, and inorganic acids and bases.

The fact that there is considerable variability in commercial sources of SDS demonstrates the need for strict quality control. Specifications for SDS purity were suggested and currently available materials were identified that match those specifications.

Problems that surface as a result of variable SDS preparations include variations in molecular weight determinations, changes in banding patterns, variable staining of bands, differences in background staining, diffusion of minor bands, and in some cases, the appearance of protein bands that shifted position and were not expected to be seen in that particular position. Other problems attributed to SDS variability were enzyme

---

. . . a process of "detergent engineering" should be evaluated.

---

renaturation difficulties and inhibition because of lipophilic material being present in the SDS preparation.

Dr. Bers mentioned that autoclaving SDS was a common practice by nucleic acid chemists. However, SDS is hydrolyzed considerably by this process, rendering it useless for protein work.

Where two-dimensional electrophoretic analysis or molecular weight determinations are part of an experiment, it is most likely that a highly purified and highly reproducible SDS preparation will be required. In cases where better resolution is required, and it is known that contaminants enhance the resolution, a pro-

cess of "detergent engineering" should be evaluated. That is, known "contaminants" need to be added in known amounts to an SDS preparation to achieve the proper results.

Dr. Steven Spotts, LKB Corp., discussed possible approaches to the standardization of isoelectric focusing using ampholytes. Companies that manufacture ampholytes try to ensure reproducibility by producing large batches and to minimize variations by carefully controlling the synthesis and subsequent fractionation thereof. Companies also distribute application notes or protocols for their particular ampholytes in an attempt

---

The end goal is to reproduce identical pH gradients from one run to another.

---

to optimize the separations process. Attention is given to electrolyte solutions, gel thicknesses, and recommended concentration of the ampholytes. The end goal is to reproduce identical pH gradients from one run to another. Problems that can arise from inhomogeneous samples, impurities in additives such as urea or other detergents, or impurities in the sample itself were also discussed.

Commercially available pI marker proteins seem to be useful for calibrating pI gradients, but they must be used while fresh. Otherwise, artifacts may arise as the proteins age. Attendees were warned against calibrating pI gradients by direct measurements because of the variabilities resulting from temperature differences. Calibrating the electrodes at 25 °C, and measuring at 4 °C can cause errors of up to one-half of a pH unit.

Immobilized pH gradients recently have been introduced as commercial products to provide powerful methods for protein separation. Because of sample-dependent properties that need to be defined, immobilized pH gradients are not ready to be considered as viable standards for electrofocusing.

Mr. William Gorman, EC Apparatus Co., detailed the current status of the industry's attempts to provide standards for electrophoresis power supplies. He considered a number of variables that could be addressed. Among those that appeared to be the most important were: 1) type of output: DC, pulsed DC with programmed decay, pulsed half-wave or full-wave rectified, or pulsed with filtering; 2) safety features; 3) types of readout; 4) output connections; 5) temperature operating ranges; 6) power style: line frequency type or switched frequency; 7) end point detection; 8) degree of regulation; 9) set point controls; 10) testing parameters; 11) serviceability; and, 12) electrical code compliance.

Mr. Gorman's talk provided an important list of

points for manufacturers to consider as newer devices are built that take advantage of increased voltages in electrofocusing.

Dr. Muriel Jansson, Image Analytics, talked about a new laser-based densitometer that is designed to scan wet two-dimensional gels and autoradiograms with high resolution. The instrument accomplishes digitization of the protein images using a 12 bit analog-to-digital converter to provide 4,096 gray levels. This device is able to scan a gel and provide all of the integrated data in about 30 minutes. The device automatically finds the spots of protein on a given gel, gives a printout of spot number, the coordinates, and the integrated total volume of each spot. It also produces correlations and matching between spots in different gels. It has a wide absorbance range that is linear up to 3 absorbance units and shows 0.1% scattering.

Dr. Catherine Phillips, DuPont, spoke on detection and quantification of radioactive proteins in gels using new autoradiographic methods. Using a commonly available video-based system, she found that there was a curvilinear relationship between spot volume and concentration of proteins stained with Coomassie Blue stain. The laser-based system, previously described by Dr. Jansson, provided a linear response between the amount of stain and the amount of protein in the stained gels. Nevertheless, fluorometric and autoradiographic methods for protein detection still proved to be more sensitive. The accurate quantification of protein and peptide "spots" in a two-dimensional gel are much more problematic. This is due to the nonlinear relationship of the photographic density generated by

---

... the need for particle standards will become increasingly important.

---

radioactivity of labelled proteins. Dr. Phillips described software to transform image data into uniformly-spaced gray levels correlated with the amount of radioactivity present in the protein. In addition, she described optimization of the image recording system by use of an astrophotographic process termed "hypersensitization" of the photographic emulsion.

Dr. Phillips concluded her talk by discussing the evidences that calibration and step tablets are essential in standardization of the electrophoretic quantification process.

Dr. Robert Snyder, National Aeronautic and Space Administration (NASA), presented information on particle standards for continuous flow electrophoresis. This technique of free-flow electrophoresis is best applied to the separation of cells and large molecules. The major difficulties in achieving reproducibility in flow electrophoresis are ascribed to buoyancy and convection perturbations. Disturbing forces can occur when temperature gradients of 0.1 °C exist.

Dr. Snyder summarized electrophoresis experiments performed in space over the history of the NASA programs. The early experiments showed the sensitivity of the electrophoresis separations to fluid viscosity changes due to electroosmosis. Cells were separated on a variety of space missions as parameters for electrophoretic separations in space were determined.

Polystyrene latex beads were separated by continuous flow electrophoresis into homogeneous fractions. Dr. Snyder suggested that as this work progresses, the need for particle standards will become increasingly important.

The meeting concluded with a roundtable discussion on directions for standardization, with Dr. R. C. Allen, Dr. Douglas Gersten, Dr. Marvin Lasky, and Dr.

The complexities and usefulness of standardization were realized ...

David Sammons as participants. Presentations focused on the current status of protein molecular weight markers and the potential for new markers for isoelectric standards as well as molecular weight markers.

In summary, the workshop was useful in bringing to light several approaches to standardization in electrophoresis. Various manufacturers of electrophoretic equipment and chemicals are interested in providing materials that will meet the needs of researchers who are extending the capabilities of electrophoresis into the analysis of smaller amounts of sample with better precision.

The complexities and usefulness of standardization were realized by the participants. Several attendees expressed willingness to be involved in a trial to test interlaboratory comparability in electrofocusing. The initial study is scheduled to begin this year as an interlaboratory round-robin to test the effectiveness of rehydratable gels for obtaining consistent patterns with standard protein preparation. NBS will serve as the coordinator and provide data analysis to determine the potential of such studies. Dr. Allen will prepare the rehydratable gels and a standard protein will be supplied by NBS.

262